MINISTRY OF TECHNOLOGY

AERONAUTICAL RESEARCH COUNCIL
REPORTS AND MEMORANDA

An Experimental Investigation of the Interaction between a Forward-Facing Step and a Laminar Boundary Layer in Supersonic, Low-Density Flow

by

E. W. E. ROGERS, C. J. BERRY and MISS B. M. DAVIS

LONDON: HER MAJESTY'S STATIONERY OFFICE

1967

PRICE 19s. 6d. NET

An Experimental Investigation of the Interaction between a Forward-Facing Step and a Laminar Boundary Layer in Supersonic, Low-Density Flow

by

E. W. E. ROGERS, C. J. BERRY and MISS B. M. DAVIS

Reports and Memoranda No. 3506*

January, 1965

Summary.

Tests have been made in the N.P.L. low-density tunnel at stream Mach numbers (M_0) near 2 on a pressure-plotting flat plate with forward-facing steps. The step heights varied between 0·1in. and 0·9in., and the steps could be traversed along the plate surface to vary the distance from the leading edge Three stream static pressure levels (p_0) were chosen: 30, 50 and 70 microns of mercury, giving Reynolds numbers per inch between 98 and 281.

. Initially the flat plate without step was investigated and it is shown that the pressure increase caused by the thick, rapidly-growing boundary layer could be estimated reasonably well over the front part of the plate by a tangent-wedge theory. Over the rear part of the plate this estimate was too high. Near the front of the plate the viscous interaction effect was in broad agreement with other tests at $M_0 = 4$ if the correlation was made in terms of the hypersonic parameter χ. The plate boundary layer was explored with a small pitot tube and its growth with distance from the leading edge was found to correspond to a simple law of familiar form. The approximate velocity distribution within the boundary layer was also deduced and is shown to be similar to the theoretical profile for a laminar boundary layer on an insulated plate at $M_0 = 2$.

The effect of a step was to increase the plate pressure between some upstream position (the interaction point) and the step itself. The incremental pressure distributions have been analysed and it is shown that the largest pressure rise (which occurs at the step) is determined almost entirely by the ratio of the step height (h) to its distance from the leading edge (L). The length of the interaction, only one or two boundary-layer thicknesses, was found to be largely independent of step position (provided the interaction point is not too near the leading edge) and proportional to $h^{\frac{1}{2}}$. With these guides it is possible to correlate the complete incremental pressure distribution for arbitrary h and L, and by dividing the incremental pressure by p_0, the effects of changes on stream pressure may be removed also. The conditions at the beginning of the interaction, local boundary-layer thickness and unit Reynolds number of the stream appear to be unimportant in themselves. The flow seems to be dominated by the step-plate geometry and the interaction is not of the 'free' type.

For large step heights, a kink develops in the otherwise smoothly rising incremental pressure distribution and it is tentatively suggested that this is evidence of an upstream effect of the reattachment process at or near the upper edge of the step. Only when the step is large compared to the boundary layer does the observed pressure-increment curve separate out into its constituent parts – a basic 'plateau' pressure associated with the separation cavity and an upstream effect of reattachment. For other flow geometries, these effects merge and are not distinguishable.

The separation point upstream of the step was found very approximately by traverses along the plate surface with a backward-facing pitot tube. The cavity, like the interaction distance, is smaller in extent (relative to the boundary-layer thickness) than at higher Reynolds numbers. Its upper boundary, for one case only, was defined by forward-facing pitot traverses through the separated shear layer and cavity. The pressure rise to separation can be deduced once the separation points are known and those estimated for the few cases investigated in the present tests agree with the broad trend predicted theoretically for high Reynolds numbers and extrapolated to low-density conditions. In detail however the pressure rise to separation, divided by p_0, correlates poorly with the Reynolds number at the beginning of the interaction, a powerful parameter at higher densities. Good correlation is obtained for all step heights if the stream pressure p_0 is used instead.

In an Appendix the influence of the width of the test plate on the centreline pressure distribution is discussed and comparison made between results from the main 2 in. wide plate and from a 4 in. wide plate.

LIST OF CONTENTS

1. *Introduction.*

The present research programme of the National Physical Laboratory is concerned with the influence exerted on model forces and surface pressures by the thick, laminar boundary layers characteristic of rarefied, near-continuum gas flows. Two earlier N.P.L. reports discussed aspects of this viscous inter-action problem, for circular cones at zero incidence[1] and for circular cylinders placed normal to the oncoming stream[2]. In both cases the authors were concerned with predicting the measured pressure distribution from a knowledge of the inviscid (i.e. high Reynolds number) pressure distribution and the boundary-layer growth in the low-density flow. For attached flows away from the stagnation region reasonably good agreement could be obtained between simple viscous-interaction theories and experiment.

These investigations were of a rather preliminary nature and their scope was partly limited by some of the experimental difficulties inherent in low-density aerodynamics. A natural development of this work would be to look at the structure of a simple laminar boundary layer and its influence on the surface pressure distribution, and then to investigate the flow changes which occur when separation is provoked. This is the aim of the experiment described in the present report. A flat plate at zero incidence was used as the basic surface; separation was induced by forward-facing steps of different heights placed normal to the stream.

2. *Experimental Details.*

The experiments were carried out in the N.P.L. low-density tunnel at a nominal Mach number of two. This tunnel which is described in detail in Ref. 1, operates with static pressures between 10 and 100 microns mercury (μ) appropriate to altitudes between about 55 and 45 miles. The comparatively low supersonic stream Mach number was chosen because the nozzle characteristics were known more precisely than at the other operating Mach number (4) and because the useable core of the flow was larger.

The basic model consists of a flat plate, having a sharp leading edge, of length 3·45 inches and span 2 inches. Along the centreline of this plate are 18 pressure holes, which are connected *via* the plate under-surface to the thermistor manometer bank[1]. The most rearward pressure hole is 2·6in. from the plate leading edge and this fact, together with the need to have some plate surface on which to rest the step gives a maximum useable length up to the step face of about 3·0in. Local surface pressures are recorded as galvonometer readings, and then converted to microns of mercury by means of calibration curves.

The nozzle diameter at the model position is about $7\frac{1}{2}$ inches and it follows that the plate spans only a small part of the nozzle. Hence it is possible that the flow on the plate may not approximate very closely to two-dimensional conditions. This situation is to some extent unavoidable. With a larger-span plate the flow in the nozzle test region deteriorates and large axial pressure gradients appear as the nozzle boundary-layer growth is distorted. The 2-inch-span plate used in the present tests represents about the widest model that can be placed in the tunnel (together with transverse steps) without significant altera-tions to the stream conditions. A fuller discussion, together with some results obtained on a 4-inch-span plate, is given in the Appendix.

Though the use of this narrow plate can be justified by experimental considerations and by comparing results for 2in. and 4in. wide plates this need not necessarily imply the complete absence of three-dimensional effects. This point must be continually borne in mind in subsequent sections. However, as will be seen, the self-consistency of some of the experimental data, under conditions of changing plate-step geometry, does suggest that the three-dimensional effects may be smaller than originally feared.

A sketch of the flat plate and the various steps is contained in Fig. 1. These steps ranged in height from 0·1 inch to 0·9 inch and could be traversed along the plate, in contact with it, whilst the tunnel was running thus allowing a series of plate pressure distributions to be obtained without the need to open up the tunnel working section. The thermistor manometer was capable of dealing with a maximum of twelve pressure holes out of the 18 present on the model and hence two runs were required to obtain a complete survey. Not all the holes were in fact used for every model geometry.

3

The general repeatability of the pressure readings was about $\pm 0.5\mu$. Some holes, however, seemed to give consistently high (or low) readings, which may perhaps be attributable either to small defects in the orifice geometry or, less probably, to unusual thermistor characteristics. As will be seen, in much of the analysis the concern is with the pressure *difference* caused by the presence of the step, and these consistent errors are thereby removed.

In addition to the surface pressures on the model, the test chamber pressure, the stagnation pressure upstream of the nozzle, nozzle mass flow and, occasionally, the static pressures on the wall of the nozzle were measured. The tests were carried out at conditions corresponding to three static pressure levels in the test flow; 30, 50 and 70μ, and the jet was balanced as far as possible for these flow conditions (*see* Ref. 1). Certainly with the 2in.-wide plate in position in the working section, there was no large axial pressure gradient near the model. The plate was mounted in the tunnel so that its rear edge was at the exit of the plastic extension to the nozzle (the 'hemline' of Ref. 1). The leading edge was therefore 3·45 in. upstream of this nozzle exit.

Even in the empty tunnel, there is a change in stream Mach number as the stream static pressure varies, and this is due to alterations in the nozzle boundary-layer growth. With a model in place, the boundary-layer growth is again modified and the effective stream Mach number is changed from the empty-tunnel value. It is therefore necessary to determine by pitot-tube surveys the Mach number distribution just upstream of the model when this is in position. This was done in the present tests at all three pressure levels and for three geometric arrangements: (i) flat plate without step; (ii) flat plate with 0·5in. step placed 3in. from plate leading edge; and (iii) flat plate with 0·9in. step at a similar position. The results are plotted in Fig. 2. The influence of the step on the stream Mach number (M_0) at the plate leading edge is very small at a stream static pressure (p_0) of 50μ. There is a larger effect at 30μ and a big increase between the no-step and 0·5 in. step cases at $p_0 = 70\mu$. The differences in the shapes of the curves contained in Fig. 2 probably arise because of the slight out-of-balance conditions induced by the step, and corresponding changes in the boundary-layer growth upstream and near the model position.

It is convenient to regard the flow Mach number as unchanged for static pressures of 30μ and 50μ, and accordingly these results are designated by the stream Mach number M_0 for the no-step case (1·92 and 2·15 respectively[†]). This procedure would not be justified at $p_0 = 70\mu$ and a stream Mach number which varies with step height has been used. The effect of step height on M_0 was determined towards the end of the experiment; the solid symbols in Fig. 2 are the initial calibration values for the no-step condition, and these agree very well with the subsequent measurements.

The plate was carefully aligned to be at zero geometric incidence throughout the tests. Because reliance has to be placed on the difference between pressure readings taken for different geometric configurations and some time necessarily elapsed between the sets of readings, great care was required both in resetting the model correctly in the tunnel and in reproducing accurately the flow conditions in the test section, particularly nozzle mass flow and the reference static pressure. The stagnation temperature (T_0) of the flow was atmospheric. Because of the need to allow time for the tunnel vacuum pumps to settle down before useful observations could be made and because the tunnel subsequently was allowed to run continuously, all readings are taken with zero heat-transfer between the flow and the model.

Based on the plate-alone stream Mach numbers deduced from pitot-traverses, the Reynolds number per inch run is as follows:

$p_0(\mu)$	M_0	Re/inch ($T_0 = 288°C$)
30	1·92	98
50	2·15	212
70	2·11	281

[†] The magnitude of the blockage effect caused by the plate alone may be judged from the fact that the corresponding empty-tunnel (or small-model) stream Mach numbers at these pressures are 2·05 and 2·19 (Ref. 1).

The work described in this report was carried out at intervals between March and September, 1964.

3. *Flat Plate without Step.*

3.1. *Pressure Distributions.*

Though the main object of the present tests was to study the effect of the forward-facing steps, it is worthwhile giving some consideration to the results obtained on the basic flat plate without a step. The local pressures on the plate surface (p_F), divided by the stream static pressure (p_0), are presented in Fig. 3. In the absence of viscous interaction arising from the thick, rapidly-growing boundary layer the ratio p_F/p_0 would be unity.

It is possible to estimate the magnitude of the viscous-interaction effect by simple approximate methods. One of these, a tangent-wedge method, was used for the present results. It was assumed that the boundary-layer growth on the plate gave a pressure distribution corresponding to a curved surface in inviscid flow, the boundary of this surface being the outer edge of the plate boundary-layer displacement thickness. This was given by the simple laminar boundary-layer equation for zero pressure gradient and zero heat transfer (*see* Ref. 4):

$$\frac{\delta^*}{x} = \frac{1\cdot73}{\sqrt{Re_L}}\left[1 + 0\cdot27\,M_L^2\right], \tag{1}$$

where δ^* is the boundary-layer displacement thickness, and Re_L and M_L are the Reynolds number and Mach number at x based on local conditions at the outer edge of the boundary layer. The slope of the displacement thickness surface, and hence the slope of the equivalent inviscid body, is given by

$$\frac{d\delta^*}{dx} = \frac{1\cdot73}{2\sqrt{Re_L}}\left[1 + 0\cdot27\,M_L^2\right]$$

$$= \tan^{-1}\phi, \tag{2}$$

where ϕ may be regarded as the local wedge angle in a tangent-wedge approximation. The flow over the wedge sections is assumed to be altered by a leading-edge shock; this has been taken as equivalent to that for a wedge joining the plate leading edge and the outer edge of the displacement thickness at $x = 0\cdot5$in.

An interation procedure is necessary to estimate the plate pressure distribution. The results compared with experiment on Fig. 4 are from the third interation; further calculations give little change in the value of p_F/p_0.

It will be seen that for stream static pressures of 30μ and 50μ, there is good agreement between theory and experiment up to $x = 1\cdot0$in. Behind this position the actual pressure on the plate falls far more rapidly than theory would predict. A similar trend was apparent in a comparison between surface pressures on cones near $M_0 = 2$ and theoretical pressures predicted from tangent-cone theory; these results are reported in Ref. 1. In both comparisons the boundary-layer equation for zero pressure gradient was used; the actual pressure gradients are quite large however and these might be expected to modify somewhat the velocity distribution within the boundary layer, and hence δ^* and the equivalent slope angle, ϕ. It may be argued however, that the differences between theory and experiment over the rear part of the plate, are just those to be expected from a boundary layer thinned by outflow over the side edges of the finite-span plate. Whilst some effect of this type is possible, the agreement between the centreline pressure distributions for the 4in. and 2in. wide plates shown in Fig. A1 suggests that this influence is largely unchanged when the span of the plate is doubled.[†]

[†] An alternative explanation is that the plate trailing-edge (at $x = 3\cdot45$in.) is influencing the upstream surface pressures and causing them to approach the free-stream value more quickly than on a semi-infinite plate.

At $p_0 = 70\mu$ agreement between theory and experiment is completely lost, and it would appear that the experimental values of p_F/p_0 are too low by about 6 per cent. This is equivalent to replacing the accepted value of 70μ for p_0 by a new value of 66μ. Though it is difficult to obtain great precision in estimating p_0 from the various measured quantities (wall pressures, stream Mach number and tunnel chamber pressure) particularly at the upper part of the tunnel operating range where the nozzle flow is not completely balanced, it seems unlikely that the actual error in p_0 is more than 1μ. The discrepancy is therefore without satisfactory explanation at present. Fortunately most of the interest in the present report is centred upon pressure changes on the plate surface due to a step and this discrepancy therefore assumes less importance. As will be seen the pressure changes suggest indirectly that p_0 is unlikely to be much different from 70μ.

The values of the ratio p_F/p_0 correlate reasonably well when plotted against $M_0/(Re_x)^{\frac{1}{2}}$, where Re_x is based on free-stream conditions and the distance x. A more interesting comparison can be made however if the hypersonic parameter $\chi = M_0^3/(Re_x)^{\frac{1}{2}}$ is employed instead, as in Fig. 5. Though its use is not entirely proper for the low supersonic Mach numbers of the present tests it does enable Aroesty's results[3] at $M_0 \simeq 4$ to be compared directly. For χ near unity the two sets of results join together; this region corresponds to the front part of the present flat-plate model. The two lines for tangent-wedge theories at stream Mach numbers near 2 and 4 confirm that agreement ought to be expected near $\chi = 1$, but the Berkeley results do not extend to low enough values of χ to shed light on the trend of the N.P.L. data as χ tends to zero. The discrepancy between theory and experiment for small values of χ is of course related to the similar disagreement apparent in Fig. 4 towards the rear of the plate.

3.2. *Boundary-Layer Growth.*

Pitot traverses were made through the boundary layer on the flat plate (without a step) at different positions of x from the leading edge and for all three values of stream static pressure. A set of five curves for $p_0 = 50\mu$ is presented in Fig. 6; for clarity experimental points are shown on only two of the curves. The interpretation of the various changes is illustrated diagramatically in the inset. The initial rapid increase in pitot reading (H_1) is due to the plate boundary layer. At some position this gives place to a much slower increase, which is assumed to be the inviscid flow region above the boundary layer but behind the leading edge shock. The slow pitot gradient suggests that the shock is curved. The edge of the plate boundary layer (δ) has been taken as the position A where the inviscid flow region starts. This region is also terminated by a fairly sudden decrease in H_1, which is followed by a zone in which the pitot pressure is very nearly constant. The latter region is the undisturbed free stream above the plate; the kink corresponds to the leading edge shock and for convenience its position has been assumed at station B in Fig. 6. Similar curves were obtained at static pressures of 30μ and 70μ, but in the former case it became difficult to define the point A on the after part of the plate because of the encroaching nozzle-wall boundary layer. The proximity of the leading-edge shock and the edge of the boundary layer for small values of x also causes difficulty at all pressure levels.

All the results shown in this section were obtained with a pitot tube of 0·048in. external diameter, 0·036in. internal diameter. Except very close to the surface the pressures recorded with this probe were little different from those obtained with a 0·125in. external diameter tube. In particular, the edge of the boundary layer was almost identical in the two cases.

The increase in δ with x at the three values of p_0 is shown in Fig. 7. The leading-edge shock for $p_0 = 50\mu$ is also drawn and the merging of this into the boundary layer near the leading edge is apparent. This shock is slightly curved, but its mean inclination is that produced by an 11 deg. wedge in the free-stream flow of Mach number 2·15. This angle is close to that used in estimating the theoretical flat-plate pressure distribution (Section 3.1 above).

The boundary-layer thickness can be correlated by plotting δ/x against $(Re_x)^{-\frac{1}{2}}$. This is done in Fig. 8 where most of the results are close to a line given by

$$\frac{\delta}{x} = \frac{7·9}{\sqrt{Re_x}}.$$

(3)

At $p_0 = 30\mu$, three points are below the curve, and this effect may reasonably be attributed to the nozzle-wall boundary layer which merges with the outer edge of the plate boundary layer at large x and makes an accurate estimate of δ difficult. The results in Fig. 8 suggest that little thinning of the boundary layer takes place over the rear part of the plate, a possible three-dimensional effect mentioned earlier.

To a first approximation Re_L in equation (1) may be considered equal to Re_x, and likewise M_0 may be substituted for M_L. For $M_0 = 2\cdot13$ (a mean value for both 50μ and 70μ conditions) equation (1) then gives

$$\frac{\delta^*}{x} = \frac{3\cdot85}{\sqrt{Re_x}} \tag{4}$$

yielding a value of δ^* which is just under one-half of the boundary-layer total thickness. Monaghan's[4] approximate solutions, with the Prandtl number put equal to $0\cdot75$, give a ratio uf δ^*/δ of about $0\cdot56$ at $M_0 = 2$. Considering the limitations of both theory and experiment in the present case, the agreement achieved is satisfactory.

3.3. Boundary-Layer Profiles.

In view of the lack of knowledge of boundary-layer structure in low Reynolds number flows, it seems worthwhile to analyse further some of the pitot-pressure distributions obtained in the present tests. Because the pitot probe is small, the viscous corrections to its reading become rather large and an iteration procedure is required to deduce the Mach number distribution in the boundary layer from the measured pitot pressure and the *local* static pressure at the particular position on the plate. Once the Mach number distribution is known however it is easy to reduce this to a velocity distribution by using Monaghan's[4] approximate analytical expressions for local temperature and velocity. The boundary layer is assumed to be without heat transfer and under zero pressure gradient. The former assumption is quite justified; the latter is not except insofar as the analysis is made much easier. The use of more complicated numerical methods (such as those described in Ref. 5, Ch. 7) involve further iterative calculations and for the present preliminary measurements the extra accuracy in the outer part of the boundary layer is probably not worth the increased computation.

The boundary-layer velocity ratio U/U_L, where U is the velocity within the layer and U_L the value at the edge of the boundary layer is plotted against $y(Re_L)^{\frac{1}{2}}/2x$ in Fig. 9 for five values of x. There is a small, but progressive, change in the boundary-layer profile with increasing x; part of this variation may be attributed to the rising local Mach number along the plate surface, and part may be associated with the local pressure gradients which are most intense near the front of the plate. At $x = 2\cdot5$ in., the boundary-layer profile is not far from that predicted by Van Driest[12] for an insulated flat plate at $M_0 = 2$. It should be remembered of course that there are several uncertainties in the derivation of these experimental velocity distributions. For example the viscous correction to the pitot-probe reading within the boundary layer is not known accurately; near the bottom of the boundary layer the Reynolds number based on tube diameter may be less than unity, and it is in this range that existing viscous corrections are scanty and moreover show some independent influence of Mach number. In addition, the effective tube displacement (due to shear) and the interference induced by the solid wall are unknown in the present conditions and have had to be neglected.[†]

Though the results shown in Fig. 9 should therefore be regarded as approximate and preliminary, it would seem that the exploration of thick, low-density boundary layer is not too difficult, provided the probe performance is well established. Because an understanding of the thick laminar layer is fundamental to progress in low Reynolds-number aerodynamics, more careful studies of the boundary-layer characteristics are planned.

[†]Because the accuracy of the velocity profiles is not very good, no attempt was made to determine δ^* from these and hence to check the value of δ^*/δ derived in Section 3.2.

4. Effect of Forward-Facing Steps.

4.1. Pressure Distributions.

The prime purpose of the present experiment was to study the influence of forward-facing steps of various heights on the plate pressures and the boundary-layer characteristics. Eight step heights (h) were tested, ranging in 0·1in. intervals from 0·1in. to 0·9in., with the exception of 0·8in., which was omitted. Steps of greater height than 0·9in. cause a progressive distortion of the flow in the region of the model, and the value of the data obtained becomes increasingly doubtful. The steps could be traversed along the plate surface (in contact with it) whilst the tunnel was running and accordingly pressure distributions were measured over a range of distances (L) between plate leading edge and step position. Generally, values of L were between 0·8in. and 3·0in. The step heights were mostly comparable with the local boundary-layer thickness; in no conditions were they extremely large or very small relative to δ.

A typical example of the pressure changes caused by a step is shown in Fig. 10. When the step is 2·6in. from the leading edge the pressure rise extends upstream to the position $x = 0·8$in. Ahead of this interaction point, the pressure readings are unchanged.

Principally, we shall be concerned with the pressure *increment* (Δp) caused by the step. This is the difference between the two curves in Fig. 10, and may conveniently be made non-dimensional through division by p_0. A set of such curves, for all eight values of h, and selected values of L, is presented in Figs. 11a to h. The stream static pressure is 30μ. For any particular step height the trends are clearly defined; as the step approaches the leading edge, there is a steady increase in the largest value of Δp which is obtained just upstream of the step. This particular value of Δp will be referred to as the corner pressure increment and designated $(\Delta p)_c$. The general shape of the pressure distribution does not alter greatly until the influence of the step reaches the plate leading edge.

At constant step position, there is a progressive rise in $(\Delta p)_c$ as the step height increases. A typical set of curves is contained in Fig. 12. The interaction distance upstream from the step also grows, but for step heights near 0·4in. the curve shape changes from one having a long 'foot' of only slowly-changing pressure to one where the pressure rise is more uniform with distance.

Before considering these results in more detail, it is necessary to discover the effect of changes in free-stream static pressure (p_0). Some of the curves (not the data points) of the various parts of Fig. 11 have been transferred to corresponding sections of Fig. 13. Data points for stream pressures of 50μ and 70μ have then been superimposed. In general the agreement between the three pressure levels is close, and is remarkably good for small values of h. In this range one may conclude that Reynolds number has only a small influence on the interaction. The length and shape of the interaction and the corner pressure rise ratio are therefore independent of the boundary-layer thickness either at the step itself or at the beginning of the interaction, a rather unexpected result.

For the larger values of h, the agreement is still good in the initial part of the pressure rise, but nearer the step differences do occur. At the highest pressure, for example, the pressure increases less rapidly as the step is approached. The most characteristic changes however are evident in Fig. 13h where a 'kink' in the pressure curve becomes more evident as the stream pressure rises.

Some of these aspects, and their implications, will now be considered in more detail.

4.2. Corner Pressure Rise.

Fig. 12 suggests strongly that there is a simple relationship between the corner pressure increment caused by the step $(\Delta p)_c$ and the step height h. In addition the various parts of Fig. 11 indicate that there is another direct connection between $(\Delta p)_c$ and the step position (i.e. L). In fact very good correlation for all step heights and positions can be achieved by plotting $(\Delta p)_c/p_0$ against the simple parameter h/L, as in Fig. 14a for which $p_0 = 30\mu$. There is a sequence of data points for each value of h and in general they lie close to a single mean line, with regions of overlap. Provided the ratio h/L is the same the pressure rise of a small step near the front of the plate is similar to that for a larger step further back. Similar degrees of correlation can be obtained at the other two stream pressures. The mean lines for all three cases are compared in Fig. 15. For small values of h/L, there is little effect due to changing p_0. When h/L is large however, the 50μ and 70μ diverge from that for $p_0 = 30\mu$, and this is another aspect of the

8

pressure differences apparent in Fig. 13h. Apart from this change at one end of the test conditions, which is discussed again in Section 4.6, it would seem that the corner pressure increment ratio† $(\Delta p)_c/p_0$ is determined only by the model geometry and is little effected by local or unit Reynolds number, or boundary-layer thickness in relation to the step height.

In view of the small part played by free-stream pressure, or step position alone in determining the corner pressure rise, it seems clear that the present interaction is not of the 'free' type, i.e. one which is basically independent of the solid boundary provoking the flow separation. This matter is discussed below in Section 4.5.

The simplest method of approximating to a pressure rise depending only on h/L is to assume that the increase is associated with a flow deflection $\tan^{-1}(h/L)$ at a given M_0. This is clearly an unrepresentative model of the real flow, but as Fig. 14 shows, it affords a standard by which to judge the actual pressure rise.

4.3. *Interaction Length.*

The various parts of Fig. 13 show very clearly that the upstream influence of the step is unaffected by changes in p_0. For a given step height the length of the interaction appears to change only slowly as L alters. To look into the aspect more closely it is necessary to define the length of the interaction, the distance a in the upper part of Fig. 16. For convenience the interaction was assumed to begin when $\Delta p/p_0$ exceeded 0·025. At $p_0 = 30\mu$ this corresponds to a pressure change of $0\cdot75\mu$, about the smallest quantity detectable with some certainty. Defined in this way the interaction distance is plotted against L for various step heights in Fig. 16. The points all lie to the right of a diagonal line $L = a$; in this limit the interaction starts at the leading edge of the plate. Though there is some scatter, particularly for small values of h, it was noticeable that a decreases only slowly as the step moves forward, until the interaction point comes close to the leading edge. The major influence on a is the step height. The data for $h = 0\cdot3$in. (and also that for $h = 0\cdot4$in., not shown in Fig. 16) do not fit in very well with the other results, and this may be attributed to the long 'foot' developed for these values of h, and which is apparent in Figs. 11c and 12. No satisfactory explanation of this phenomenon can be advanced.

The arrangement of the curves in Fig. 16 suggest that any dependence of a on L is not linear. Indeed for a given value of L, and providing the interaction point is not close to the leading edge, the interaction distance is roughly proportional to $h^{\frac{1}{4}}$. Fig. 17 shows that apart from the 'odd' points near $h = 0\cdot4$in., the same correlation line is valid for all three values of p_0. The actual numerical constant would vary a little as L changes. Once again the independance of the interaction length from boundary-layer thickness (or unit Reynolds number) must be stressed.

The interaction lengths shown in Fig. 16 are only one or two boundary-layer thicknesses in extent, and this is strikingly different from conditions in high Reynolds number flows where the interaction usually starts tens of boundary-layer thicknesses upstream of the disturbance. Chapman, Kuehn and Larson[6], using an argument which should be accepted with caution for the low-density interaction, show that the ratio a/δ^* depends inversely on the square root of the surface-friction coefficient at the interaction point, i.e. directly with $Re_i^{\frac{1}{4}}$. As Re_i decreases, so does a/δ^*. Though this dependence is not apparent locally within the limits covered by the present tests, it is consistent with the much smaller interaction length for low-density flows; a reduction of Re_i from 10^6 to 10^2 would give a tenfold decrease in interaction length, about the amount observed.

4.4. *Correlation of Complete Pressure Distribution.*

It has been established that the corner pressure rise caused by the step can be correlated by a single line, dependent on the geometric ratio h/L (Fig. 14a). In addition Figs. 16 and 17 suggest that the interaction length a is approximately proportional to $h^{\frac{1}{4}}$ and that a is largely independent of L.

---

† This ratio is of course equivalent to a conventional pressure coefficient C_p at constant M_0.

These aspects lead to the possibility that the complete pressure distribution upstream of the step can be correlated if the length distance $(L-x)/h^{\frac{1}{2}}$ is used, and the pressure scale is approximated by N, where

$$N = \frac{\Delta p}{p_0} \cdot \left(\frac{L}{h} \right).$$

This assumes of course that the curve in Fig. 14a can be replaced by a straight line. A correlation of this type for varying step heights but fixed L is shown in Fig. 18. The free-stream static pressure is 30μ. The general agreement between the sets of points is quite good, though there is some divergence at the step itself, $(L-x)/h^{\frac{1}{2}} = 0$, partly because of the rather crude linear approximation to the curve of Fig. 14a. The data for $h = 0.2$in. do not correlate well because of the error in assuming for this case that $a \propto h^{\frac{1}{2}}$ (see Fig. 17). Moreover, for small step heights, the scatter in the original data is magnified by the method of presentation, and this is particularly noticeable near the beginning of the interaction. Nevertheless Fig. 18 demonstrates the underlying unity of the pressure variation upstream of the step. Similar Figures may be plotted for the other two stream static pressures and for different values of L.

The type of comparison made in Fig. 18 may be extended slightly by comparing a number of incremental pressure distributions at different values of L and h. A typical comparison of this type is shown in Fig. 19. Again the correlation is satisfactory.

The data in Fig. 19 cover a wide range of L/h and clearly similar agreement could be achieved at a constant value of this ratio. This raises an interesting point. The correlation in Fig. 19 is *dimensional*, and to make it non-dimensional the abcissa needs to be divided by the square root of a length. If it is accepted that the incremental pressure distributions should be capable of description in *non-dimensional* terms, then this characteristic length should be associated in some way with the experiment. Clearly the length cannot be connected with the model geometry, since alterations in x, a, L or h would destroy the correlation. Moreover, this length cannot be associated with mean-free path, because this depends on p_0, and the correlation, though plotted for simplicity at one pressure in Fig. 19, is independent of p_0. The only remaining length in the experimental system would seem to be associated with the viscous-induced pressure gradient over the plate, and could be considered in terms of the distance (J) required for unit change in p_F/p_0. J should of course be smaller at the lowest stream static pressures where the induced-pressure effects are largest. However Fig. 3 suggests that over the front part of the plate at least the gradient of p_F/p_0 is not very different for the three test conditions. If this is accepted, then J may provide the missing dimension in Fig. 19; such an explanation is not completely convincing however.

4.5. Significance of Geometric Correlation.

It seems quite clear that the pressure disturbance imposed by the step is dominated by the plate-step geometry. Hence the interaction is not of the 'free' type where a large part of the pressure-rise curve is independent of the surface shape causing the interaction. These systems have been discussed in detail by Chapman, Kuehn and Larson[6] for moderate supersonic Mach numbers and by Miller et al[10] and Erdos and Pallone[11] for hypersonic flows. They show by simple order-of-magnitude arguments that the 'free' type of interaction is governed by boundary-layer conditions at the interaction point and to a smaller extent by the local Mach number at this position. If it is accepted that free-interaction arguments apply to the whole of the incremental pressure distribution then in the present case[+] the maximum pressure rise should depend mainly on $(Re_i)^{-\frac{1}{4}}$. More specifically Ref. 11 suggests that at $M_0 = 2$

$$\frac{p_c - p_i}{p_i} = \frac{3 \cdot 5}{Re_i^{\frac{1}{4}}}. \tag{5}$$

[+] Strictly, the free interaction arguments apply to the forward part of the pressure distribution, but in the present tests it is convenient to use p_c which is linked geometrically with the rest of the incremental pressures.

This ratio has been evaluated for a selection of step heights and positions at $p_0 = 50\mu$ and the results are plotted against Re_i in Fig. 14b. For a given step height the pressure ratio $(p_c - p_i)/p_i$ is almost constant and hence largely independent of Re_i; the dominant influence is clearly step height itself. All values fall below those predicted by equation (5), though as the step increases the observed values approach the broken line. From this one might argue that equation (5) is a limiting case where the boundary layer is very much smaller than the step, a situation common in the high Reynolds number flows which form the background to 'free-interaction' analyses. Indeed the main difference between the present results and those obtained at higher Reynolds numbers (Refs. 6, 7) perhaps lies in the fact that for the low-density results the steps are comparable with, or less than, the boundary-layer thickness. At higher Reynolds numbers the steps are frequently much greater than the boundary-layer thickness, though there is some evidence in Ref. 7 that the step height, when this is small, affects the maximum pressure rise even at high Reynolds numbers. Ref. 11 also mentions the possibility of small steps producing inter-actions which are not of the free type. One is tempted therefore to speculate that the corner pressure rise may well be linked (say) to the distribution of total pressure within the approaching boundary layer. Even more crudely the pressure rise due to the step might be proportional to the pitot pressure in the undisturbed plate boundary layer at the position later to be occupied by the upper edge of the step. These pitot pressures have of course been measured and are plotted in Fig. 6 for $p_0 = 50\mu$. Since $(\Delta p)_c$ depends only on h/L, it might be hoped that the pitot pressure at (say) $x = L = 2 \cdot 0$ in. and $y = h = 0 \cdot 4$ in., (point C in Fig. 6), would be similar to that at $x = L = 1 \cdot 0$ in. and $y = h = 0 \cdot 2$ in. (point D). In fact the pressures are not exactly the same, and the difference is increased if the local static pressure, p_F, has to be subtracted to achieve a clear comparison with $(\Delta p)_c$. Except for $x = 0 \cdot 5$ in. (which is not required, fortunately, in the present argument about $(\Delta p)_c$), the boundary-layer traverses made through the inner part of the boundary layer (say $< 0 \cdot 8\delta$) collapse reasonably well if an ordinate y/x is used in place of y, indicating that the pitot pressure depends significantly on y/x or for the purposes of the present argument, h/L. Because the correlation fails completely when the upper edge of the step is above the undisturbed boundary-layer edge, it might be accepted that the pressure rise is controlled by conditions inside the boundary layer at a distance smaller than h from the plate surface, and even by some average condition.

Here then, on rather vague terms, is a possible mechanism for the strong h/L dependence observed in the results. If it is accepted, then according to Fig. 6, we should expect $(\Delta p)_c$ to increase more or less linearly with h at constant step position (Line EE'). Fig. 12 confirms this prediction. Alternatively if a given step is traversed along the plate the corner pressure increment will rise rapidly (Line FF'). Again this is in accordance with the results presented in Figs. 11 and 13.

This argument does not at once dispose of the difficulty that the *same* pressure increment ratio $(\Delta p)_c/p_0$ is obtained for a given step with *different* static pressures and hence boundary-layer thicknesses. It is significant perhaps that even with the different-sized profiles obtained at the three stream pressures, within the inner part of the boundary layer the ratio H_1/p_0 is achieved at about the same physical distance from the surface at a given x. This ratio is presumably the most relevant one.

The foregoing arguments are aimed at showing why the corner pressure rise (and through this the general incremental pressure distribution) is sensitive to the geometric ratio h/L. It does not explain why the length of the interaction is independent of p_0 but increases almost as $h^{\frac{1}{2}}$. Indeed no really satisfactory explanation of this phenomenon can be put forward; most order-of-magnitude arguments linked to the structure or growth of the laminar boundary layer suggest that the interaction length should be proportional to h, or even some higher power of the step height. Clearly a fuller understanding of the basic interaction mechanism is needed.

4.6. *Pressure-rise Curves for Large Step Heights.*

It was mentioned in Section 4.1 that distinctive differences between the shape of the pressure-increment curves occur at the largest step heights and that these differences alter with p_0. This can be seen in Fig. 13h. The most noticeable feature is the 'kink' which develops in the incremental pressure distribution and which is particularly pronounced at $p_0 = 70\mu$. At the lowest test pressure (30μ) the kink is only just apparent for $h = 0 \cdot 9$ in., and does not appear at $h = 0 \cdot 7$ in. (Fig. 11g). A full set of the incremental pressure

distributions for $h = 0.9$ in., $p_0 = 70\mu$ is contained in Fig. 20. The kink appears to start at about 1 in. upstream from the face of the step at all values of L; at lower pressures this distance is slightly smaller.

In high Reynolds number flows there are two distinct types of phenomenon which give rise to pressure distributions similar to those in Fig. 20. It may occur when transition to turbulent flow takes place in the separated shear layer upstream of the step. In this case the increased mixing in the transitional layer superimposes a rapid pressure rise on a laminar pressure distribution which has a long constant-pressure 'plateau' region (*see* Ref. 6). There was no direct evidence that transition was occurring upstream of the step in the present tests and it seems highly unlikely at the very small Reynolds numbers of the flow. Secondly a plateau followed by a pressure rise may occur with a wholly laminar layer if reattachment takes place; this has been demonstrated many times for disturbances like wedges, but for steps the effect appears not to have been noticed, presumably because reattachment always takes place on or near the upper edge of the step and this does not influence the cavity pressure.

Clearly this general flow pattern with reattachment on the step must be true also in the low Reynolds number flow. The pressure rise to reattachment may however penetrate upstream and so influence the local pressures *ahead* of the step particularly if the cavity is not large compared with the boundary-layer thickness. Ref. 1, for example, demonstrates that the expansion round the rear shoulder of a circular cone may influence the pressures on the cone surface well upstream from the corner; presumably this upstream penetration is proportional to local boundary-layer thickness and would not be very evident in high Reynolds number flows. The curves of Fig. 20 may thus be formed of two components, as sketched in Fig. 21. There is a basic 'plateau' distribution,[†] and to this must be added the upstream contribution due to reattachment. If the boundary-layer is 'thin', as at $p_0 = 70\mu$, the upstream penetration is insufficient to mask all the plateau and a kink develops. If the pressure is reduced so that the boundary layer is thicker the result is a smooth (but composite) pressure distribution.

If the foregoing argument is accepted it follows that all the 'smooth' pressure-movement curves for smaller values of h are in reality formed from the two basic elements. Possibly even for small step heights, the reattachment pressure rise predominates, though this seems unlikely. More probably the basic 'plateau' distribution moves continually to the face of the step over the relatively small cavity, and when the reattachment pressure is added the resultant kink is smoothed naturally by viscous mixing effects. It only becomes manifest when the step height, and reattachment pressure rise, are large. In these cases it might be expected that the corner pressure ratio $(\Delta p)_c/p_0$ would no longer be independent of p_0 and Fig. 15 shows that there are marked discrepancies between the 50μ and 70μ curves on the one hand and the 30μ curve on the other at high values of h/L. There are points where this concept of the upstream penetration of reattachment effects runs counter to the arguments for the strong dependence of $(\Delta p)_c/p_0$ with h/L put forward in Section 4.5. This dependence, it was suggested, was a consequence of the geometric similarity of the inner boundary-layer profile at different values of x. However, it is the *total* pressure rise which results from the penetration of the step into the boundary layer. How the total rise is apportioned between that developed above the separation cavity (the so-called 'plateau' pressure) and the upstream penetration effect is a matter for internal balance. Both events would be strongly influenced by the value of H_1/p_0 at the station occupied by the upper step edge.

5. The Separation Cavity.

5.1. The Separation Point.

It has been tacitly assumed in the preceding Section that separation does of necessity take place upstream of the step. Though it seems highly unlikely, it is possible to imagine a flow model where the thick boundary-layer adjusts itself to flow up the forward face of a small step, leaving only a vestigial remnant of 'stagnant' flow in the corner of plate and step. This would not be in accord with the accepted

---

[†] The word 'plateau' is used here and in Fig. 21 in a rather loose sense. The pressure contribution due to the separation cavity may not actually become constant above the cavity; it is sufficient that the rate of pressure change is rather less rapid than near the separation point.

model of a cavity having reattachment of the upper edge of the step and pronounced reversed flow towards some separation point upstream of the step. It seemed imperative then to determine the position of this separation point for the present models.

The detection of flow separation in a low-density tunnel is no easy matter however. Surface flows of light oils or dust were tried with no success. Argon afterglow flow visualization does not show boundary-layers very clearly, and separation cavities are not distinguishable. Despite intensive efforts the pressure levels proved (as expected) too low for conventional, but very sensitive, schlieren and schlieren-interferometer techniques to give useful information.[†]

It was therefore decided to determine the separation point by traversing a backward-facing pitot tube along the plate surface. Very crudely, it may be argued that in the region of attached flow the pitot tube will give a reading smaller than the local static pressure (due to the base flow over the orifice) and in the reversed flow, the probe will record a pressure higher than the local surface pressure. Separation, therefore, takes place when the pitot pressure equals the local static pressure. This conclusion is modified slightly by considering the effect on the pitot reading of the transverse gradient, the possible shape of the separation cavity, and the low Reynolds number of the measurement. Clearly, at best the method is an approximate one, but it may serve for the present investigation to give comparative estimates of the separation point.

Traverses of this type were taken for $L = 3 \cdot 0$in. at all three static-pressure levels for step heights of $0 \cdot 3$in., $0 \cdot 5$in. and $0 \cdot 7$in. An example of the results obtained is shown in Fig. 22; the separation point is here assumed to be near $x = 1 \cdot 6$in., about $0 \cdot 4$in. downstream of the interaction point. The results of the complete investigation are shown in Fig. 22. The data, for the $0 \cdot 3$in. step were unsatisfactory at $p_0 = 30\mu$ and have been omitted. For a given static pressure, the line joining the separation point and the upper edge of the step has about the same slope (β). This line may be regarded as the first approximation to the edge of separation cavity.

5.2. The Separation Cavity Boundary.

Ref. 8 contains results of computer calculations for the cavity shape generated by forward-facing steps on flat plates near $M_0 = 2$, at Reynolds numbers (Re_i) appropriate to conditions at the interaction point between $1 \cdot 1 \times 10^4$ and $2 \cdot 4 \times 10^5$. The slope of this cavity boundary just after separation (β_1) is plotted in Fig. 24 against Re_i. Also shown on this Figure is β_2, the boundary slope measured experimentally[6] when the cavity is well-developed. β_2 is far smaller than β_1 and is more comparable with the average slope values β of Fig. 23. These are also plotted against Re_i in Fig. 24 and seem to be reasonably consistent with the high Reynolds number data, though the extrapolation from one set of results to the other is large. It is clear however that the cavity in low-Reynolds number flow is smaller (relative to the step height) and this would of course be expected from the shorter upstream effect produced by the step in low-density flow, a topic discussed in Section 4.2.

An additional attempt was made to determine the cavity boundary more precisely for one model geometry ($L = 3 \cdot 0$in., $h = 0 \cdot 5$in.) by traversing a small forward-facing pitot tube through the separated shear layer and cavity in a direction normal to the plate surface. Two such traverses are compared in Fig. 25 with similar results for the flat plate without a step. At $x = 1 \cdot 5$in., the two sets of results are in very close agreement even though the pressure interaction begins some distance upstream near $x = 1 \cdot 15$in. At $x = 2 \cdot 0$in. (not plotted on Fig. 25) there are small differences between the two curves, and by $x = 2 \cdot 5$in., these differences are very marked. With the step in position there is an outward displacement of the original boundary-layer profile, and as the surface is approached the pitot pressure begins to fall less rapidly until close to the surface a constant reading is obtained. This final change in slope (point B in Fig. 25) is assumed to correspond to the outer 'edge' of the separation cavity (assuming that this 'edge' can in fact be defined).

[†] Work is now in hand to use thin-film thermocouples to detect separation by measuring surface temperature.

Boundary points of this type were found at $x = 2 \cdot 0$in. and $2 \cdot 25$in. also and all three values are plotted in Fig. 26. They are very consistent with a cavity boundary that extends from the separation point of Fig. 23 to the upper edge of the step, and thus give some degree of confidence to the deductions made from the backward-facing pitot traverses. The pitot traverse made normal to the surface also revealed a new flow feature well above the cavity. Its approximate position is plotted in Fig. 26a and it seems to correspond to a shock caused by the thickening boundary layer just upstream of the cavity. The leading-edge shock is undisturbed by the presence of the step at least up to $x = 2 \cdot 0$in. This leading-edge shock and that associated with the boundary-layer separation can be seen in the argon-afterglow photograph contained in Fig. 26b. The darker region of the thickening boundary layer upstream of the interaction point is also visible, but the cavity is not well defined.

5.3. *Separation Pressure Rise.*

Once the position of the boundary-layer separation has been established some assessment can be made of the pressure rise required to promote separation. This topic has been discussed extensively for laminar boundary layers at high Reynolds numbers and results for $M_0 = 2 \cdot 3$, taken from Ref. 6, are indicated in Fig. 27 as a hatched band for values of Re_i between 10^4 and 10^6. The ordinate is $(p_s - p_0)/p_0$, where p_s is the pressure at separation and p_0 is the free-stream static pressure.[†] The low-density results do not correlate particularly well on this basis but they lie in the general region obtained by extrapolating Chapman, Kuehn and Larson's data to small Re_i, by means of their theoretically-predicted $Re_i^{-\frac{1}{4}}$ rule. It seems then that the low-Reynolds-number data are broadly consistent with earlier high Reynolds number results, but that for detailed correlation Re_i is not the best parameter. The latter fact is in line with remarks made in previous Sections of this report about the lack of correlation with any form of Reynolds number.

In fact the best correlation of the separation pressure-rise ratio is obtained if this is plotted against p_0, as in Fig. 27. Results for all three step heights collapse onto a single line. The parameter $(p_s - p_0)/p_0$ falls rapidly as p_0 rises and approaches the value found for high Reynolds number conditions. Because these results are for only one step position ($L = 3 \cdot 0$in.) it is not possible to estimate how universal this type of correlation is, and more work is clearly required. There is little to be gained at this stage by speculation on the significance of this correlation. It is sufficient therefore to note its existence, and also its implications in future investigations.

6. *Concluding Remarks.*

The present investigation has shed some light on the nature of the disturbance imposed on a flat plate by forward-facing steps at moderate supersonic speeds.

Perhaps the most striking feature of the analysis is the strong dependence of the imposed pressure changes on the geometry of step and plate, to the virtual exclusion of such usual parameters as boundary-layer thickness, unit Reynolds number, or local conditions at the interaction point. It has been shown that the corner pressure rise due to the step depends closely on h/L, and is nearly proportional to this ratio. The forward influence of the step, limited by the interaction point, is proportional to $h^{\frac{1}{2}}$. With these two clues to the pressure and length scales of the phenomenon it is possible to correlate the complete incremental pressure distribution from interaction point to step, for nearly all step positions, step heights and stream static pressure levels. The interaction is not of a 'free' type; the downstream geometry (step height) has a marked effect on the whole interaction.

For the largest steps a new phenomenon is apparent, and kinks develop in the incremental pressure distribution on the plate. It is tentatively suggested that these are evidence of an upstream penetration of the pressure rise associated with reattachment at the upper edge of the step, an event likely to be of

---

[†] Strictly the ordinate should be $(p_s - p_i)/p_i$ where p_i is the pressure at the interaction point. The difference is small for the high Reynolds number data, but does make some difference to the low-density results. The general link between the two régimes is unaffected however.

significance only in low-density flows with their thick laminar boundary layers. This upstream penetration must clearly exist at all test conditions to a greater or lesser extent, and it follows that the smoothly-rising incremental pressure curves found for test conditions may well be composed of two distinct features; a basic 'plateau' distribution associated with the separation cavity, and a pressure rise due to reattachment near the step.

Because of the difficulty in detecting reliably boundary-layer separation, only a limited amount of information was obtained on the shape of the separation cavity and the pressure rise to separation. The cavity is far shorter than at higher Reynolds numbers, but its shape seems compatible with consistent development from those conditions. The pressure rise to separation is roughly in accord with predictions made from high-Reynolds-number data, but the underlying correlation now seems to be in terms of free-stream static pressure rather than Reynolds number at the interaction point.

During the tests pitot explorations of the plate boundary layer were made. The growth rate when the step was absent was determined, and the velocity distribution through the layer has been evaluated in a rather approximate manner. None of this work revealed any significant departure from what might be expected in the test conditions. The results were not sufficiently accurate to warrant analysis in great detail, but they served two main purposes firstly of giving more insight into the flow about a plate-and step combination, and secondly of showing that a precise study of low-density boundary-layer characteristics is possible with only modest development of the present instrumentation. This is important, because an understanding of the laminar boundary is fundamental to the aerodynamics of bodies in low Reynolds number, continuum flows.

In brief then these tests have revealed several interesting features basic to low-density aerodynamics, besides uncovering some phenomenon and concepts worthy of further study.

LIST OF SYMBOLS

a	Interaction length, defined in Fig. 16
C	Chapman-Rubesin factor
h	Step height (inches)
H_1	Pitot pressure
L	Distance between plate leading edge and step
M_0	Free-stream Mach number at plate leading edge
M_L	Local Mach number at position x
N	$\dfrac{\Delta p}{p_0}\left(\dfrac{L}{h}\right)$
p	Pressure
p_c	Maximum pressure, reached in plate-step junction
p_F	Local pressure on flat plate without step
p_i	Local pressure at the interaction point
p_0	Free-stream static pressure
p_s	Pressure at separation
Δp	Pressure increment caused by presence of step
$(\Delta p)_c$	Maximum pressure movement at junction of plate and step
Re_i	Reynolds number based on conditions at interaction point
Re_x	Reynolds number at x based on free-stream conditions
Re_L	Reynolds number at x based on condition at the boundary-layer edge
U	Velocity in boundary-layer profile
U_L	Local velocity at outer-edge of boundary layer
w	Spanwise dimension of test plate
x	Distance from leading edge of plate
y	Distance normal to plate surface
β	Angle between plate surface and line joining separation point and upper edge of step

δ Boundary-layer total thickness

$\delta*$ Boundary-layer displacement thickness

ϕ $\tan^{-1}\dfrac{d\delta*}{dx}$

χ Hypersonic similarity parameter, equal to $M_0^3(Re_x)^{-\frac{1}{2}}$ (i.e. $C=1$)

μ Pressure equal to one micron of mercury

REFERENCES

No.	Author(s)	Title, etc.
1	E. W. E. Rogers, C. J. Berry and Miss B. M. Davis	Experiments with cones in low-density flows at Mach numbers near 2. A.R.C. R. & M. 3505. March, 1964.
2	S. C. Metcalf, C. J. Berry .. and Miss B. M. Davis	An investigation of the flow about circular cylinders placed normal to a low-density, supersonic stream. A.R.C. R. & M. 3416. April, 1964.
3	J. Aroesty	Pressure distributions on flat plates at Mach 4 and low density flow. Univ. Calif. Inst. Eng. Res. Tech. Rep. HE–150–157 (1958).
4	R. J. Monaghan	An approximate solution of the compressible laminar boundary layer on a flat plate. A.R.C. R. & M. 2760. November, 1949.
5	N. Curle	*The laminar boundary layer equations.* Oxford Mathematical Monographs (1962).
6	D. R. Chapman, ... D. M. Kuehn and H. K. Larson	Investigation of separated flows in supersonic and subsonic streams with emphasis on the effect of transition. NACA TR 1356 (1958) (*see* also NACA TN 3869).
7	J. R. Sterrett and .. .. J. C. Emery	Extension of boundary-layer separation criteria to a Mach number of 6·5 by utilizing flat plates with forward-facing steps. NASA TN D–618 (1960).
8	D. E. Abbott, M. Holt and J. N. Nielson	Studies of separated laminar boundary layers at hypersonic speed with some low Reynolds number data. AIAA Summer meeting June, 1963 (63–172).
9	K. Oswatitsch	Die Ablösungsbedingung von Grenzschichten. *Proc. of Boundary-layer Research Symposium*, Freiberg, August, 1958. Springer-Verlag (1958) pp. 357–367.
10	D. S. Miller, R, Higman .. and M. E. Childs	Mach 8 to 22 studies of flow separations due to deflected control surfaces. *AIAAJ*, Vol. 2, pp. 312–321 (Feb. 1964).
11	J. Erdos and A. Pallone ..	Shock boundary layer interaction and flow separation. *Proc.* 1962 *Heat Transfer and Fluid Mechanics Institute.*
12	E. R. van Driest	Investigation of laminar boundary layer in compressible fluids using the Crocco method. NACA TN 2597 (Jan. 1952).

APPENDIX

Effects of using a wider plate

The test plate used for all the results discussed in the main body of this report was 2in. in width and it was realized when this dimension was chosen that it was rather narrow to ensure a close approximation to two-dimensional flow over most of its length. Unfortunately a larger-span plate introduces serious blockage effects into the test section; axial pressure gradients appear both upstream and along the model. This is because the disturbances from the model (shocks, wake) after the balance between the jet static pressure and the tunnel chamber into which the nozzle discharges. It becomes difficult to judge the precise conditions for which no upstream effect from the tunnel chamber can penetrate through the thick nozzle-wall boundary layer and so influence the flow upstream of the model (the so-called balanced condition decribed in Ref. 1). Moreover the thick nozzle boundary layer is influenced directly by the model flow field and this too can alter conditions well upstream of the model. The present model span ($w = 2 \cdot 0$in.) represents a rather unsatisfactory compromise between the need to approach two-dimensional flow on the plate and the necessity of maintaining uniform stream flow in the working section.

Some checks were made in order to estimate the influence of plate width on the pressure readings. Side extensions were fitted to the 2in. plate so that its total width became 4in.; the pressure holes however still remained on the centreline. With the wider plate, the wall pressures were measured at stations 1·55in. ahead of the plate leading edge and the same distance behind it. Pitot-probe measurements were taken very close to the plate centreline in order to determine the stream Mach number distribution for 3in. upstream of the plate leading edge. All these quantitites could be compared with similar values for the 2in. wide plate.

In general, the wider plate increased the wall pressures and imposed a marked pressure difference between the two holes. The pressure immediately above the model increased sharply, whilst that upstream of the leading edge did not alter greatly. For example, with each plate in position and conditions adjusted to correspond to a free-stream static pressure of 70μ, the upstream and adjacent nozzle holes read 69μ and $71 \cdot 5\mu$ for the 2in. plate and 70μ and 79μ for the 4in. plate. The Mach number just ahead of the leading-edge of the 4in. plate was little changed (2·10 in place of 2·11). It was concluded that the simplest assumption to make was that the nozzle had become unbalanced and that the appropriate value of p_0 for the wide plate should be that for the narrow plate (70μ) augmented by the change in pressure at the nozzle wall hole immediately above the model (i.e. $7 \cdot 5\mu$). Actually a value of $p_0 = 78\mu$ was later used. Similar measurements suggested that the appropriate value of p_0 for the wide plate should be 55μ and 32μ in place uf 50μ and 30μ. The stream Mach numbers were changed from 2·15 to 2·10 (at $p_0 = 55\mu$) from 1·92 to 1·82 (at $p_0 = 32\mu$). These effective stream static pressures are of course only an approximation to the real flow conditions about the wide model.

The static pressure distribution on the wide plate was measured at all three pressure levels and then divided by the appropriate new values of p_0. These results are compared with those for the narrow plate in Fig. A1. The agreement is remarkably good, both in absolute values of p_F/p_0 and in distribution in the x direction. The former agreement may to some extent arise from fortunate choices in the values of p_0 for the wide plate. However, on this evidence it appears that the plate width has no great influence on the centreline distribution of p_F/p_0; it seems reasonable to infer that the results for the narrow plate are not too different from true two-dimensional flow.

A further series of measurements were made on the wide plate with a 0·5in. high step placed 3in. from the leading edge. The plate pressures upstream of the step were measured for the three nominal values of p_0, care being taken to repeat as far as possible the mass flow and total pressure of the runs without a step. Large differences were noted however in the pressure measured by the wall hole upstream of the plate leading edge, and hence the actual flow conditions are much more uncertain. The incremental

pressures caused by the step, however, were divided by the p_0 appropriate to the step-less plate, a procedure fully justified in the case of the narrow plate and retained for the wide plate for want of any alternative.[†]

The comparison between the incremental pressure distributions for the wide and narrow plates is presented in Fig. A2. At a nominal pressure of 30μ, the agreement is very good; at the two higher static pressures the incremental pressures are higher for the wide plate and the upstream interaction appears longer. The significance of these differences is difficult to assess in view of the rather non-uniform flow conditions in the tunnel stream. An increase in the value for p_0 at the two higher pressures would improve the agreement· for example. Moreover with the wide plate it may no longer be justified in substracting plate pressures with the step in place from those obtained in a rather different stream when the step is absent. The pressures upstream of the interaction point were not in agreement, in contrast to the narrow plate results (*see* Fig. 10), and though an overall correction has been applied for this in obtaining Δp, the correction may in reality be larger nearer the step. This too would affect the comparison. All things considered it seems reasonable to accept the narrow-plate results as at least a fair approximation to two-dimensional flow. Certainly the use of a wider plate would have given little improvement.

[†] The measured pressures at the wall hole opposite the model were influenced by the step and were not suitable for determining a new p_0.
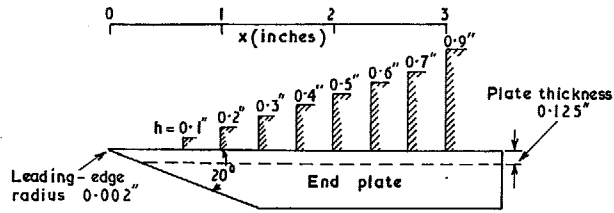
FIG. 1a. Side elevation of plate showing end plates (to isolate lower-surface effects) and steps, drawn at arbitrary distances from leading edge.
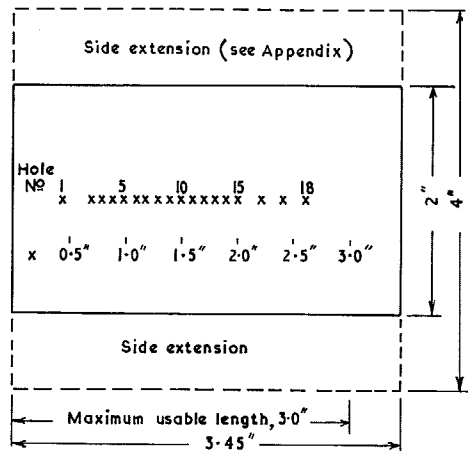
Hole Nº	1	2	3	4	5	6	7	8	9	10	11	12	13	14	15	16	17	18
x(inches)	0·45	0·7	0·8	0·9	1·0	1·1	1·2	1·3	1·4	1·5	1·6	1·7	1·8	1·9	2·0	2·2	2·4	2·6

FIG. 1b. Plan view showing pressure-hole positions and side extensions.
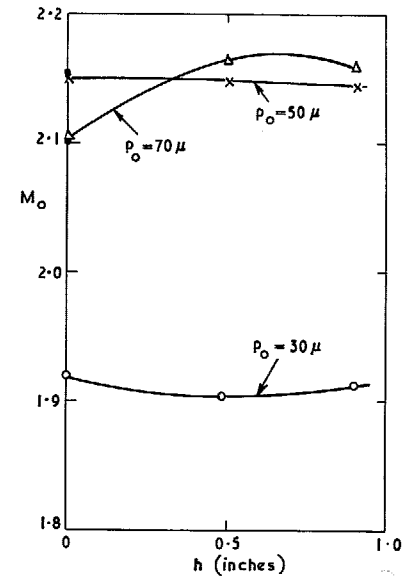
FIG. 2. Effect of step height (h) on Mach number (M_0) at leading edge of plate. (Original calibrations at beginning of test shown as solid circles).
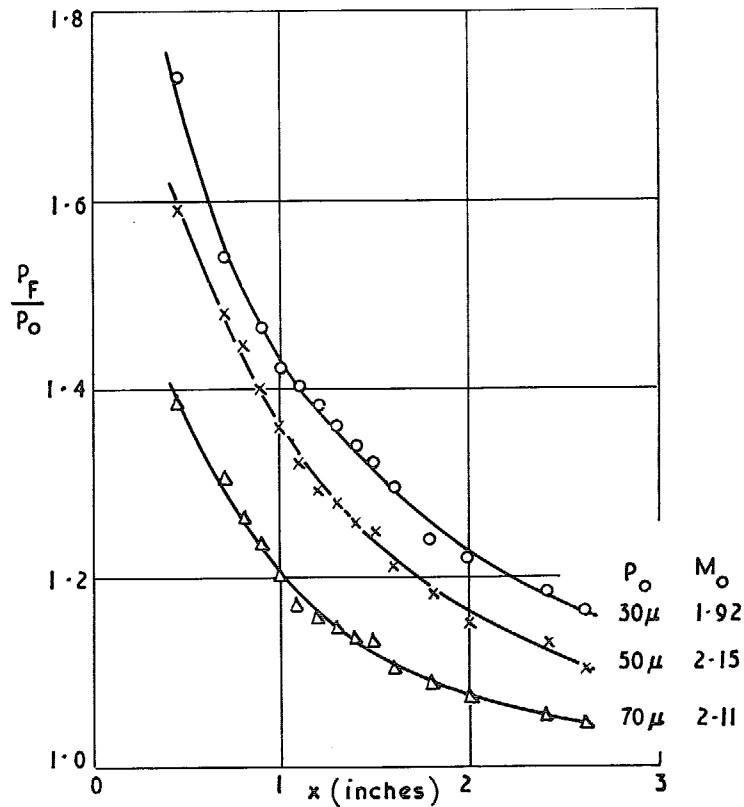
FIG. 3. Flat-plate pressure distributions on centre-line of model (2in. span).
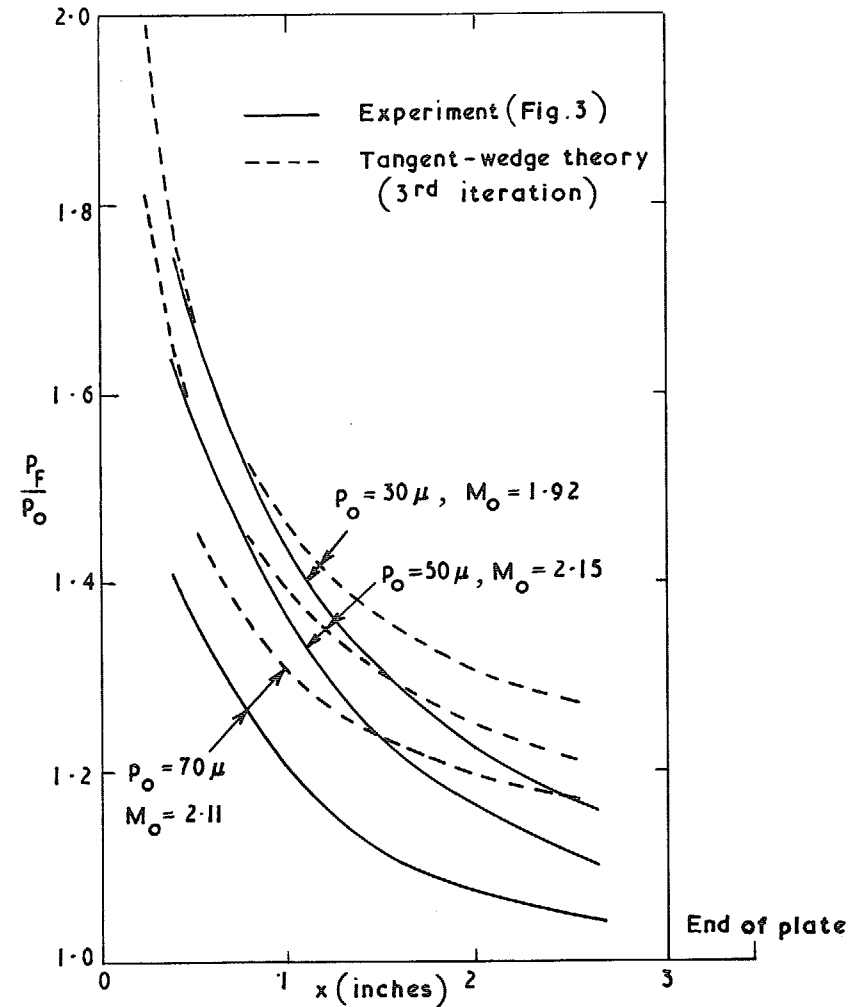
FIG. 4. Flat-plate pressure distributions; comparison between experiment and simple tangent-wedge theory.
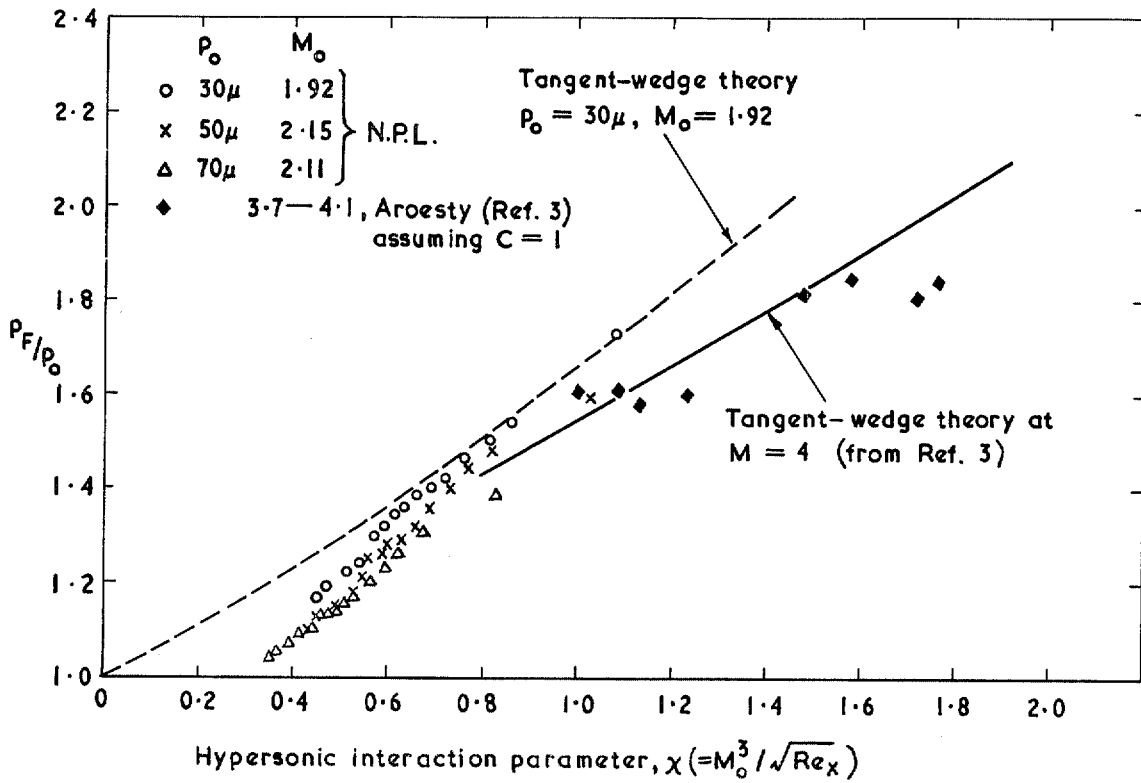
FIG. 5. Correlation of flat-plate pressure on basis of hypersonic interaction parameter.
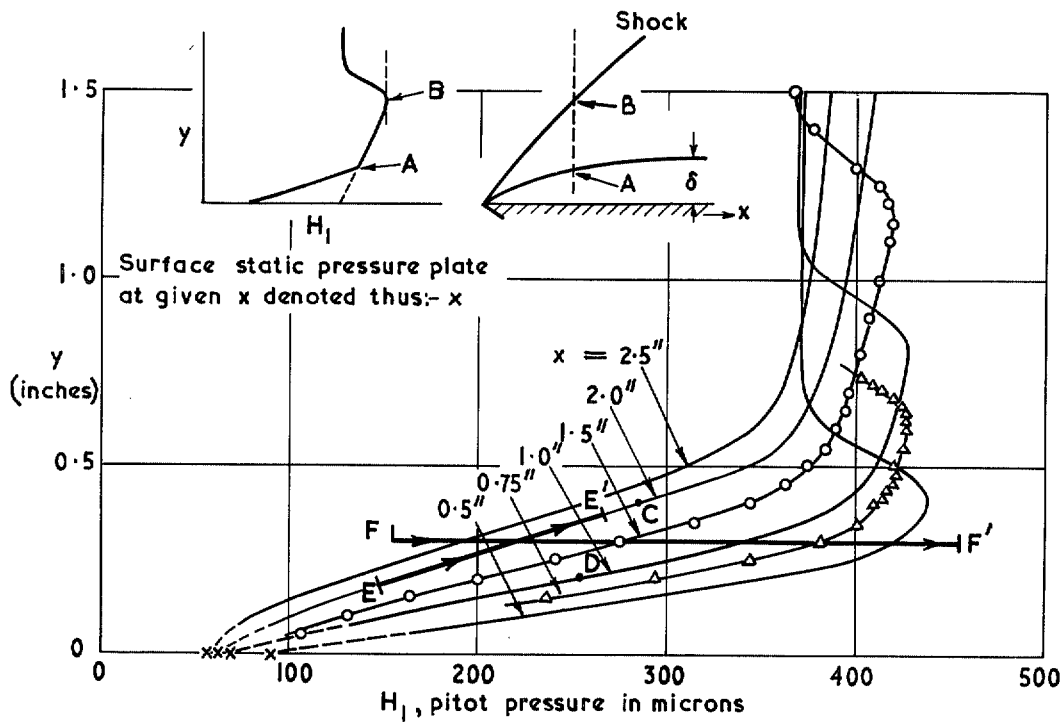
FIG. 6. Boundary-layer traverses on flat plate at $p_0 = 50\mu$, $M_0 = 2\cdot15$ (no step).
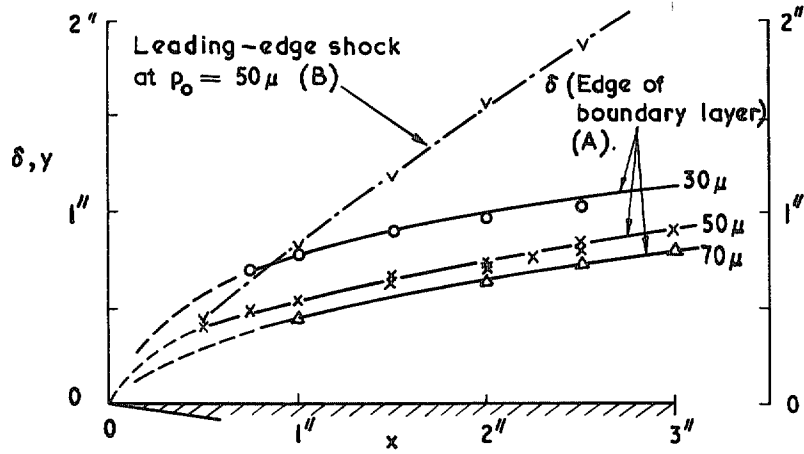
FIG. 7. Boundary-layer growth along flat plate deduced from pitot traverses (no step).
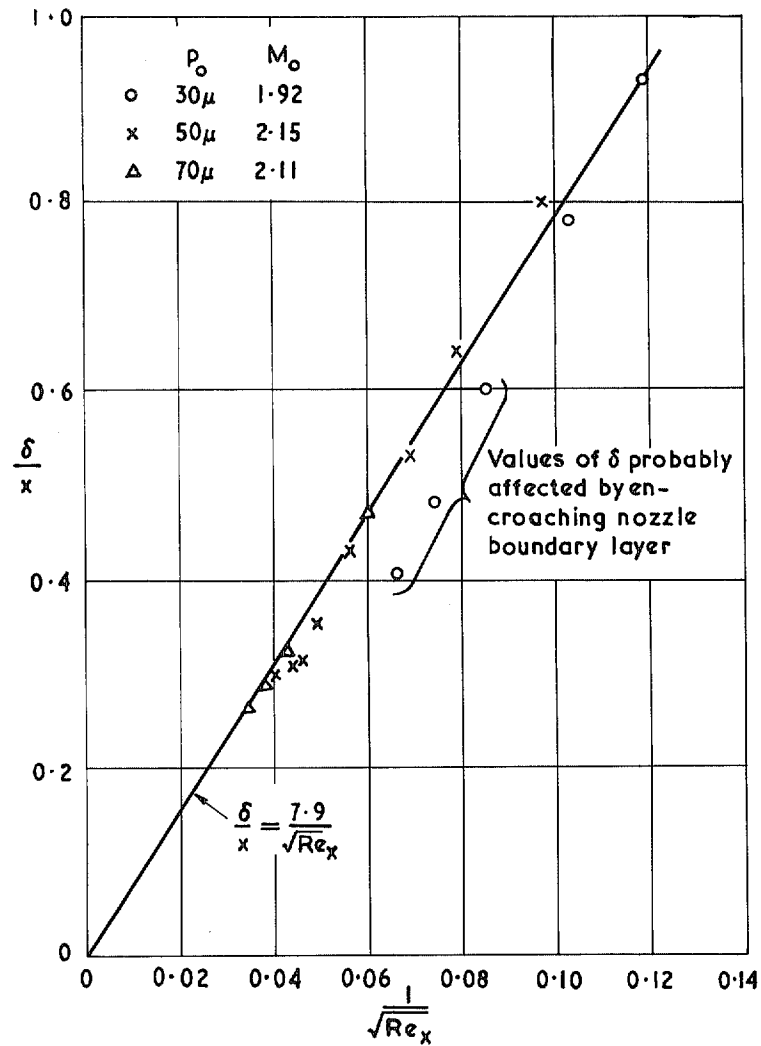
FIG. 8. Correlation of flat-plate boundary-layer growth.
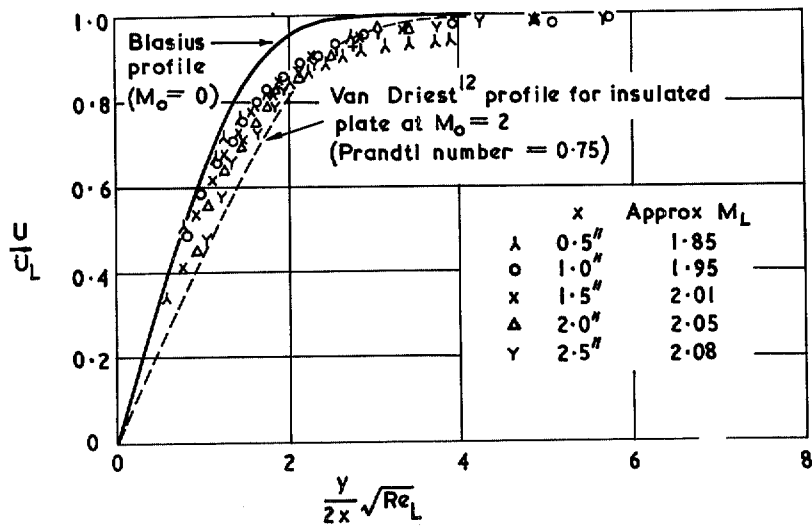
FIG. 9. Comparison of measured velocity profile with theoretical solutions ($p_0 = 50\mu$).
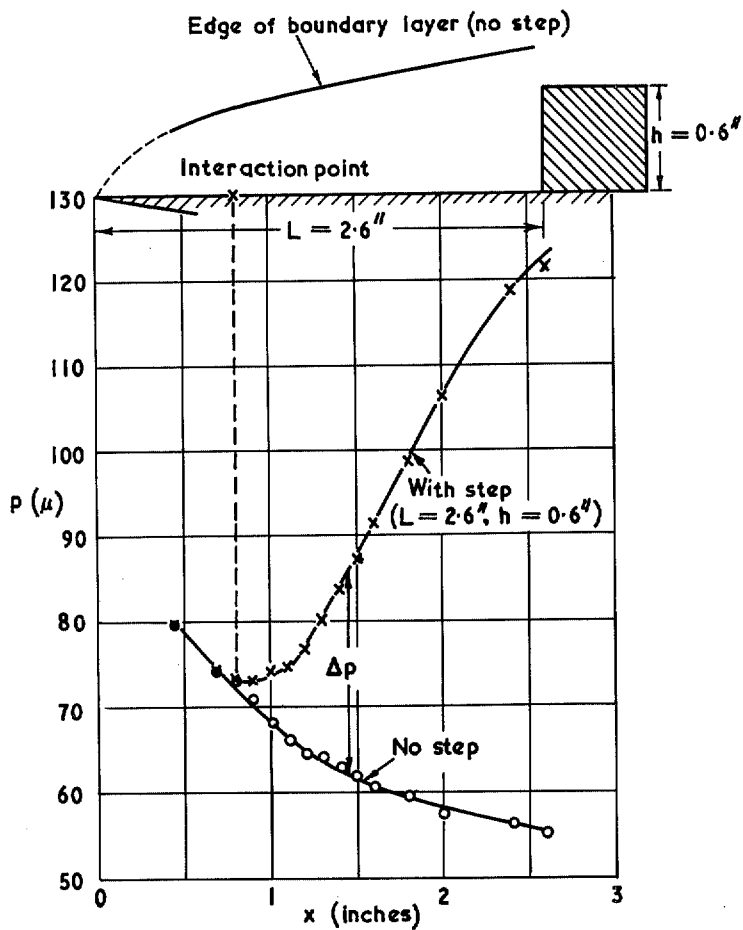
FIG. 10. Example of step influence on plate pressures at $p_0 = 50\mu$.
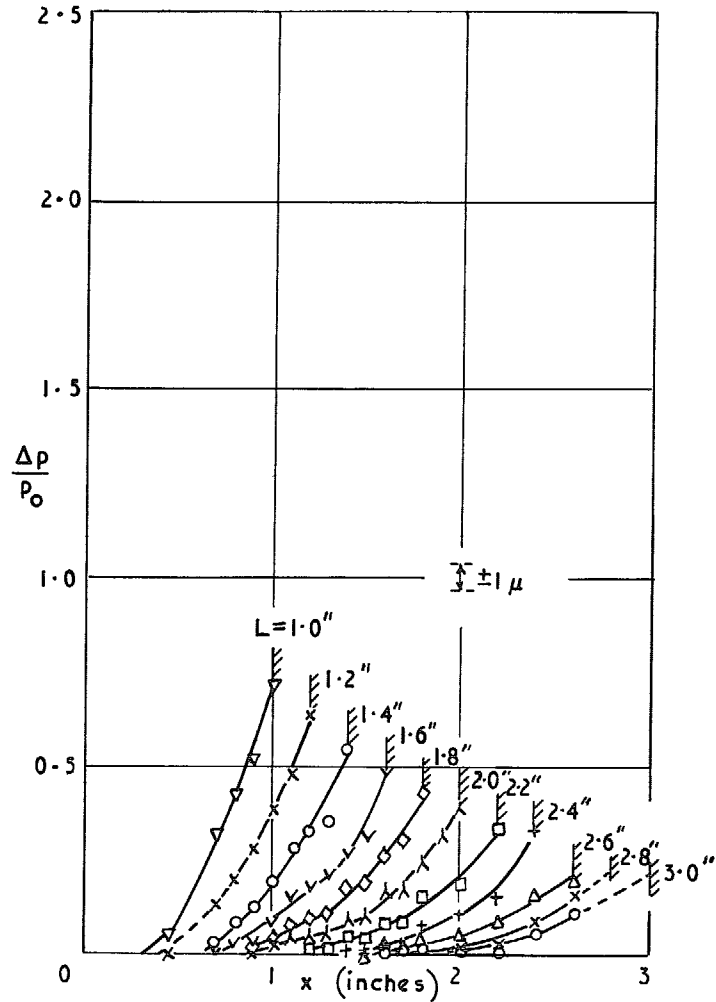
FIG. 11a.   Incremental pressure distributions for
$h = 0\cdot1$in., $p_0 = 30\mu$, $M_0 = 1\cdot92$.
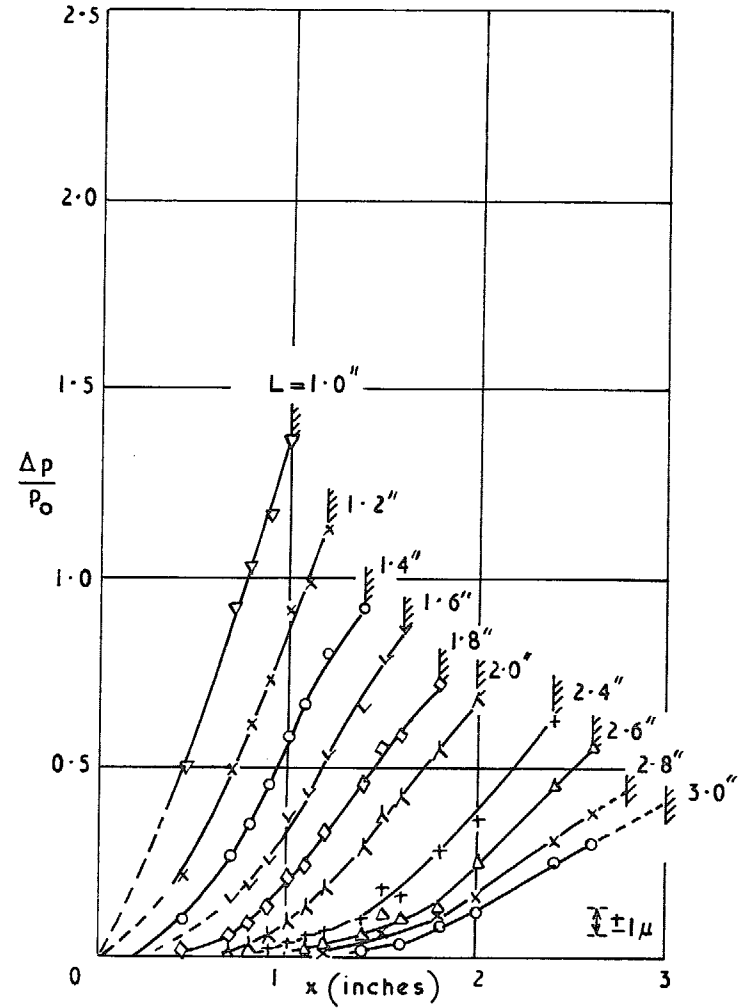
FIG. 11b.   Incremental pressure distributions for
$h = 0\cdot2$in., $p_0 = 30\mu$, $M_0 = 1\cdot92$.
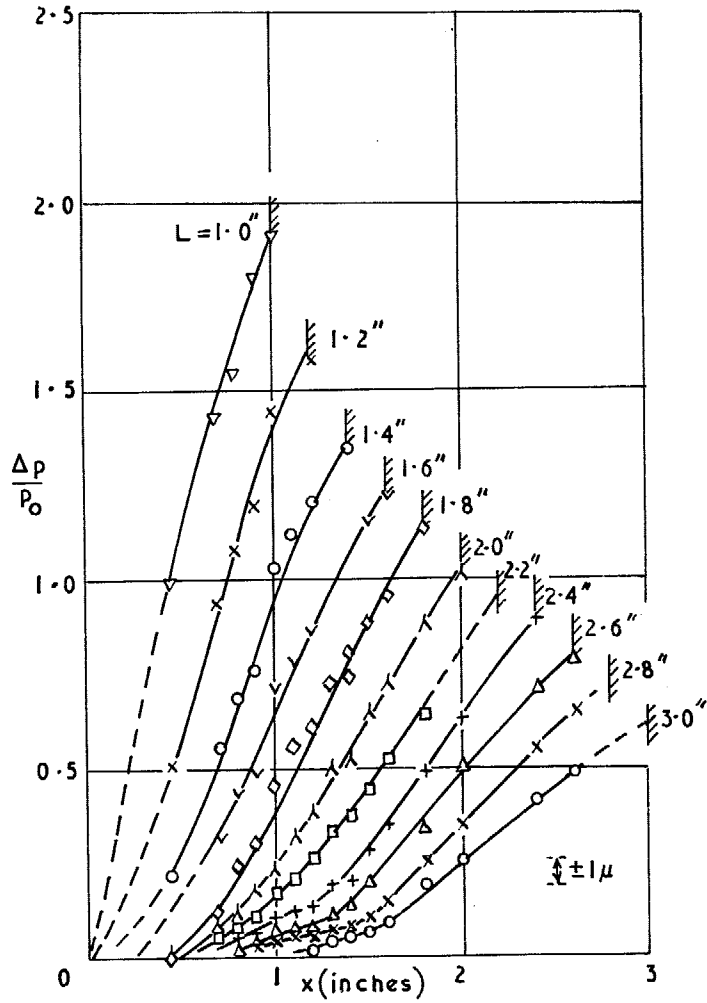
FIG. 11c. Incremental pressure distributions for
$h = 0.3$in., $p_0 = 30\mu$, $M_0 = 1.92$.
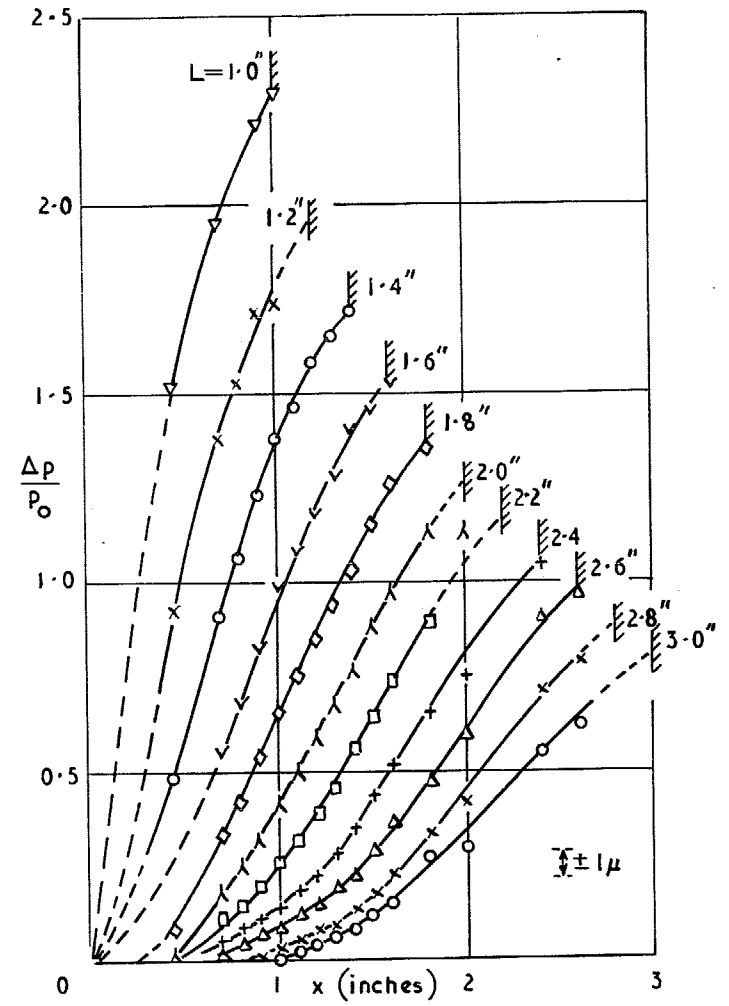
FIG. 11d. Incremental pressure distributions for
$h = 0.4$in., $p_0 = 30\mu$, $M_0 = 1.92$.
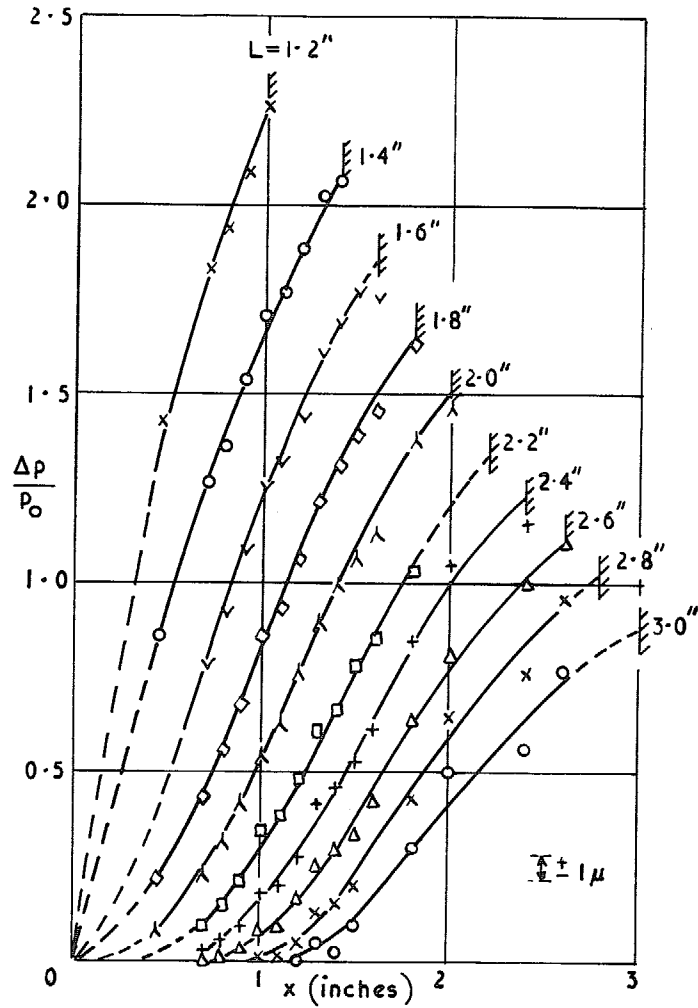
FIG. 11e.   Incremental pressure distributions for
$h = 0.5$in., $p_0 = 30\mu$, $M_0 = 1.92$.
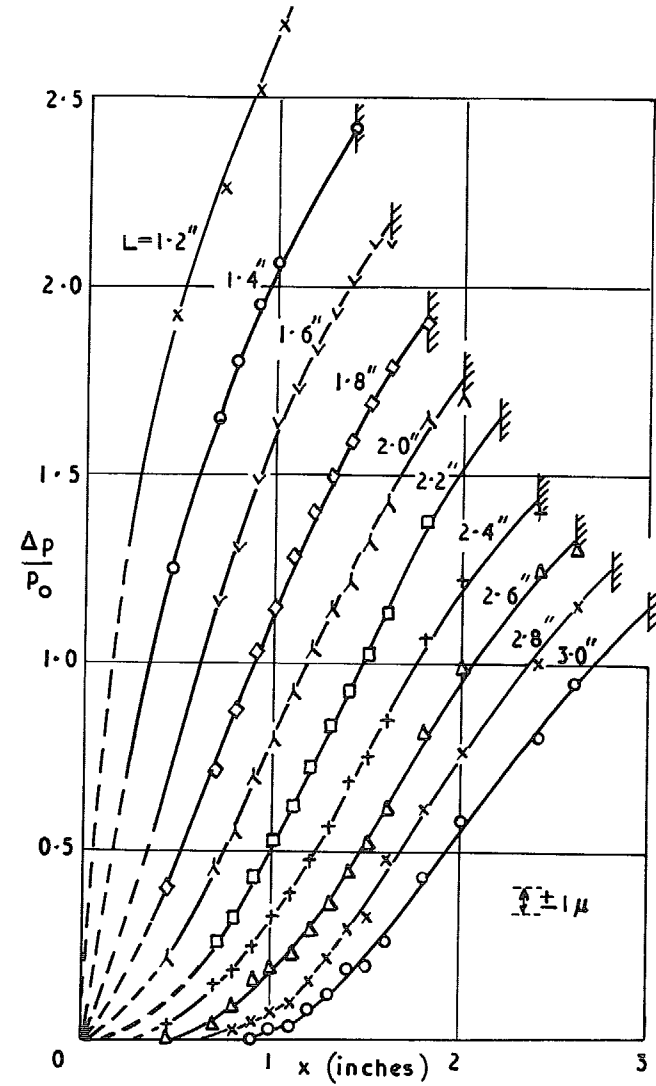
FIG. 11f.   Incremental pressure distributions for
$h = 0.6$in., $p_0 = 30\mu$, $M_0 = 1.92$.
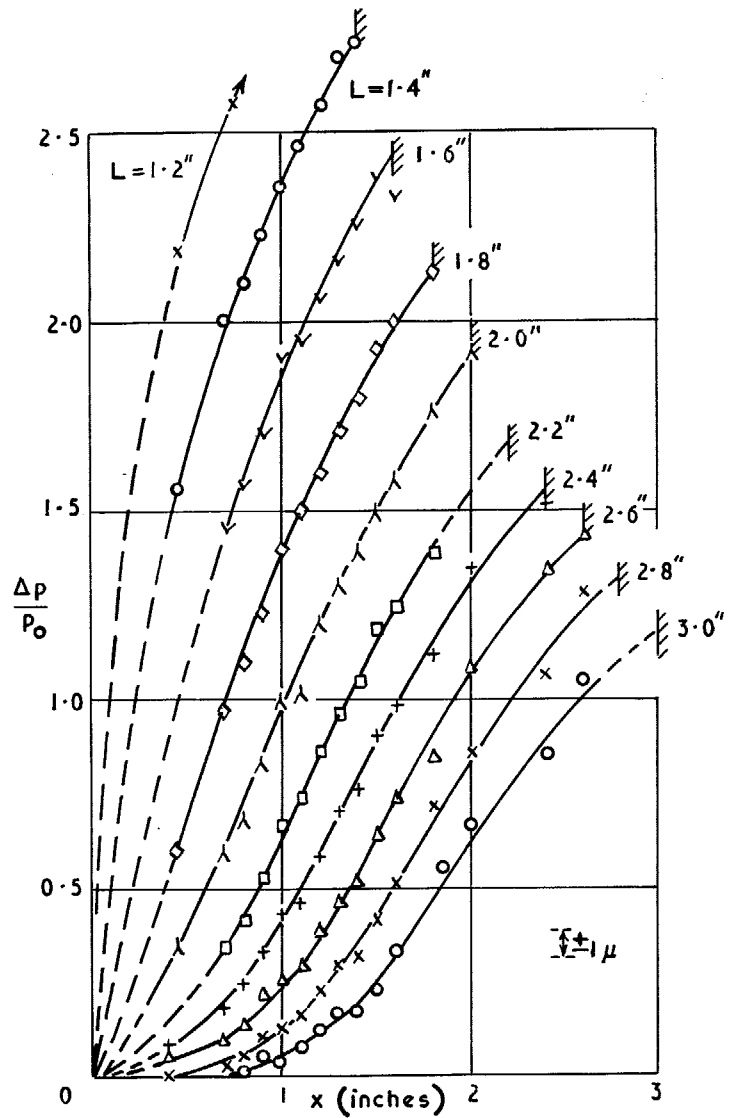
FIG. 11g. Incremental pressure distributions for $h = 0.7$in., $p_0 = 30\mu$, $M_0 = 1.92$.
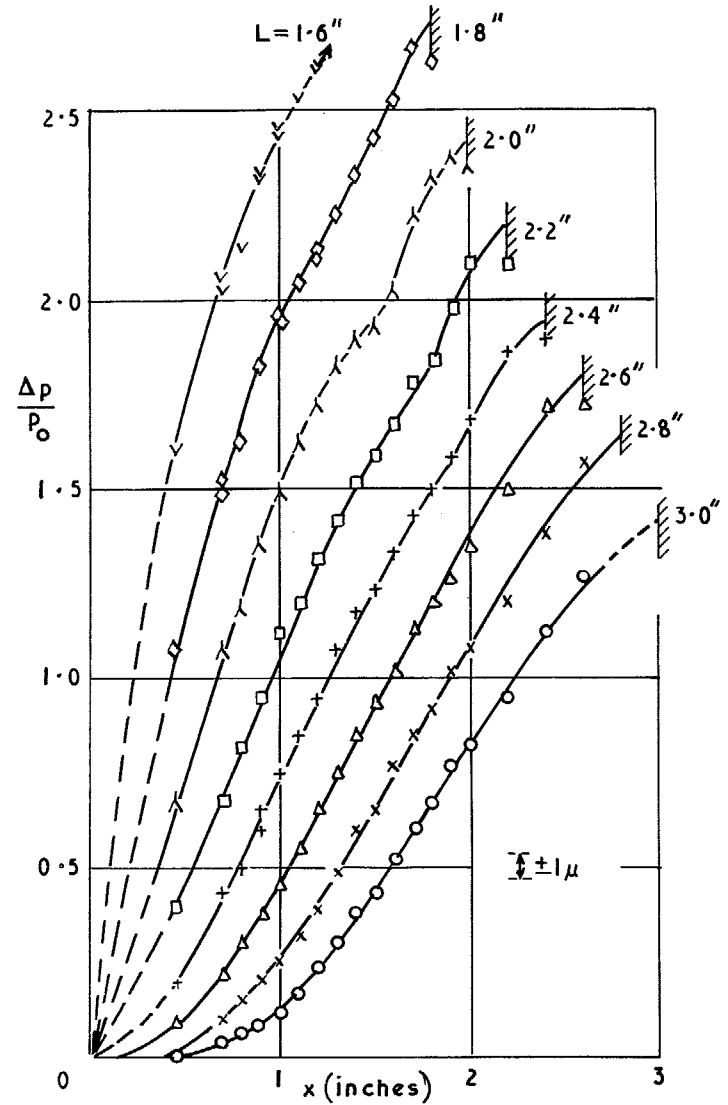
FIG. 11h. Incremental pressure distributions for $h = 0.9$in., $p_0 = 30\mu$, $M_0 = 1.92$.
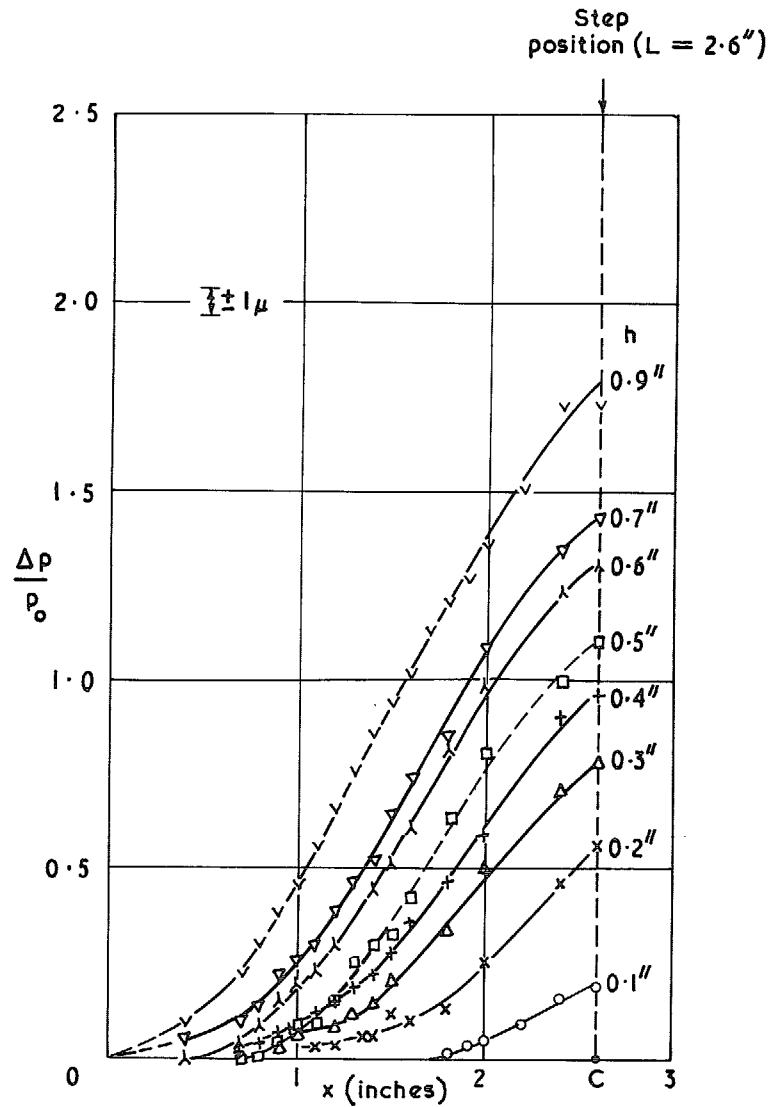
FIG. 12. Incremental pressure distributions for fixed step position and various step heights ($p_0 = 30\mu$, $M_0 = 1.92$).
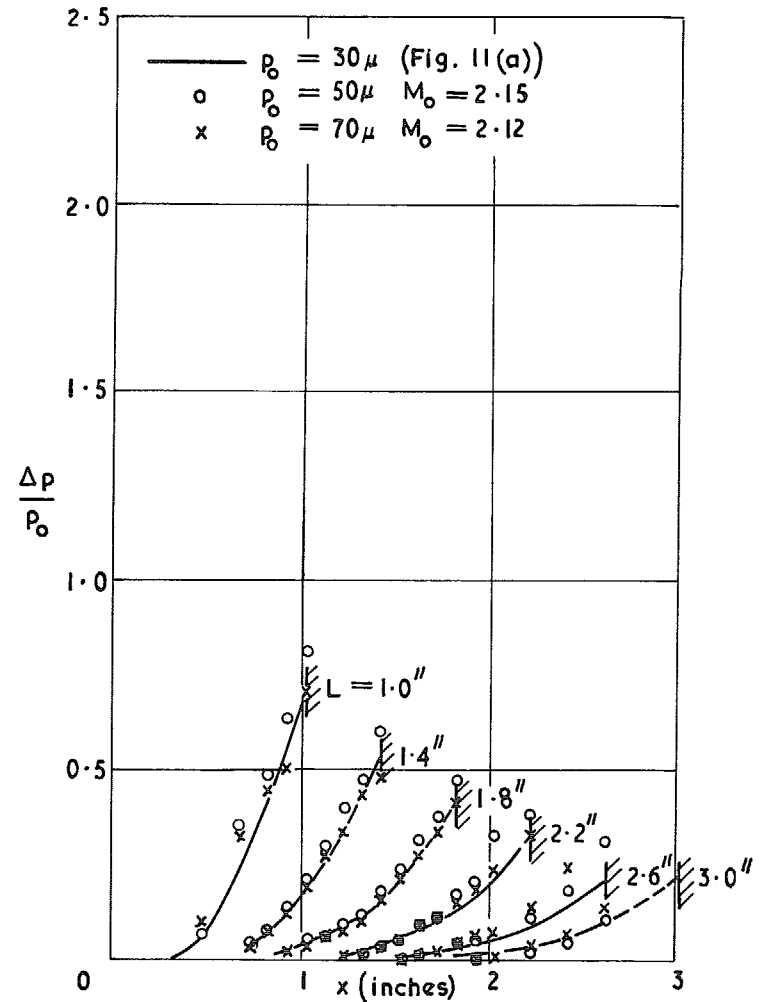
FIG. 13a. Effect of stream static pressure on incremental pressure distribution for $h = 0.1$in.
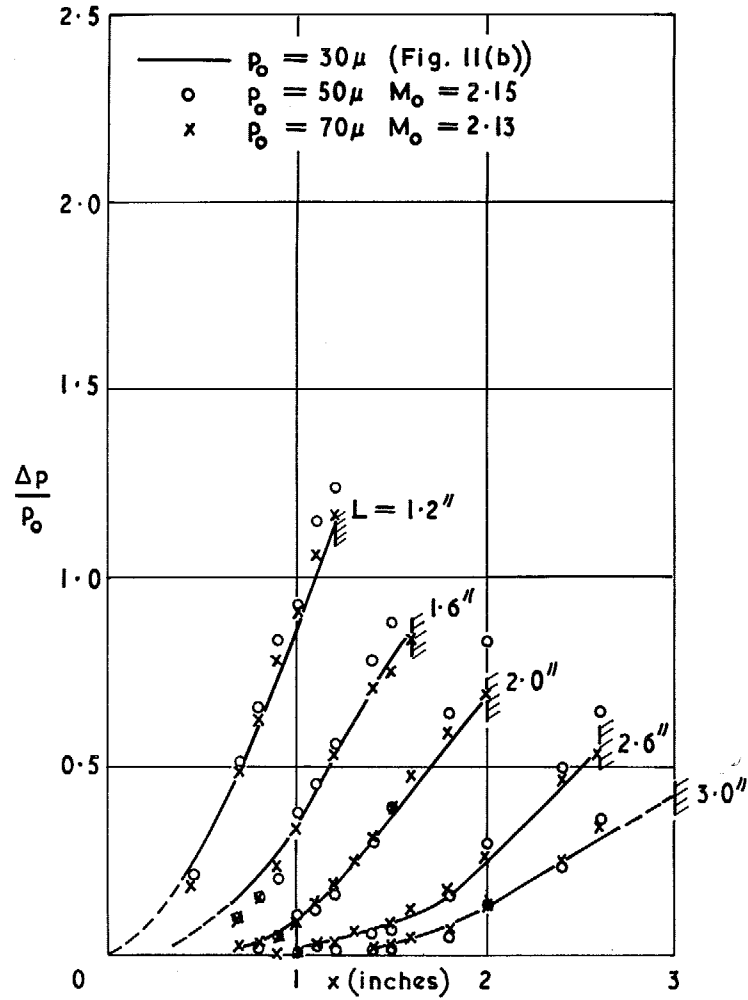
FIG. 13b. Effect of stream static pressure on incremental pressure distribution for $h = 0.2$in.
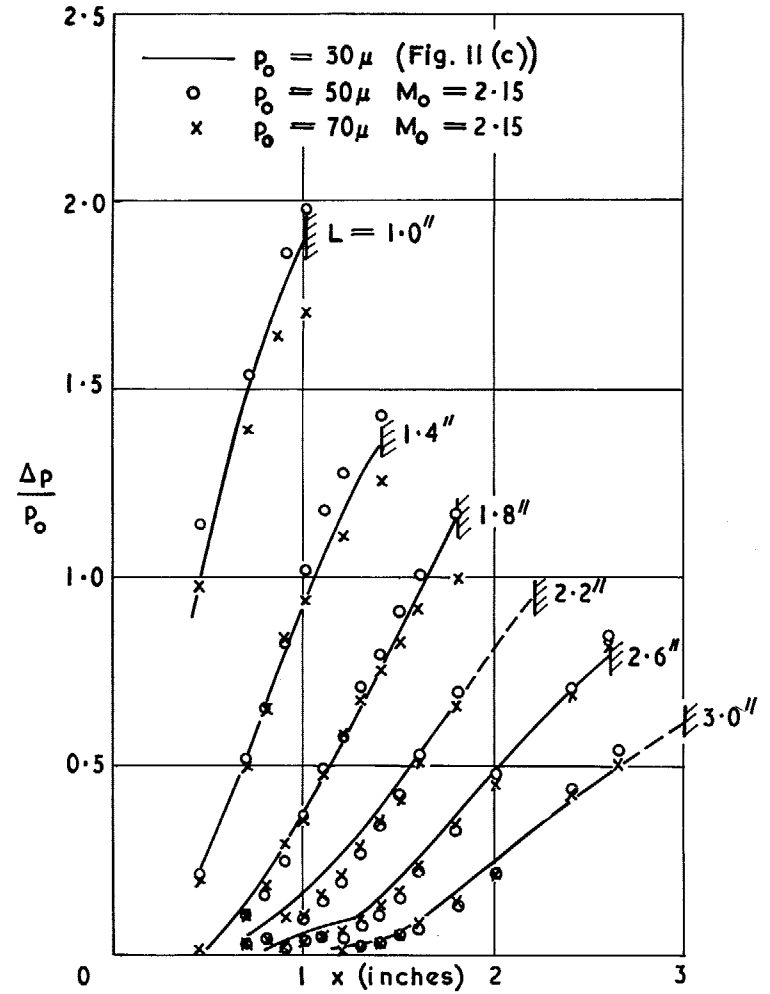
FIG. 13c. Effect of stream static pressure on incremental pressure distribution for $h = 0.3$in.
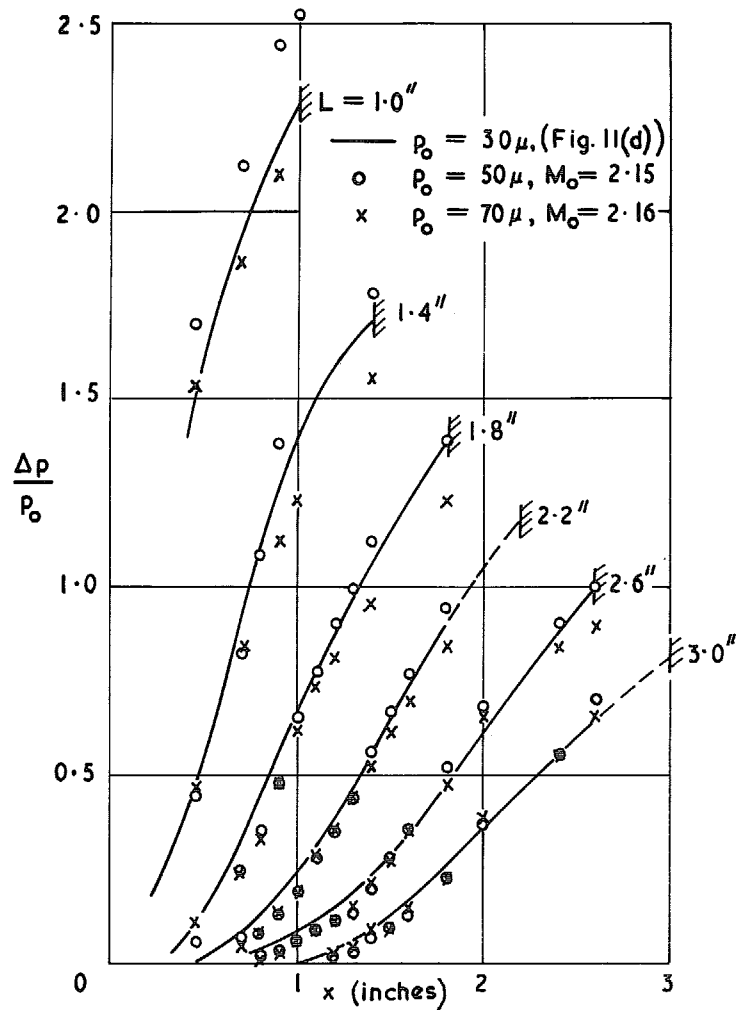
FIG. 13d. Effect of stream static pressure on incremental pressure distributions for $h = 0.4$in.
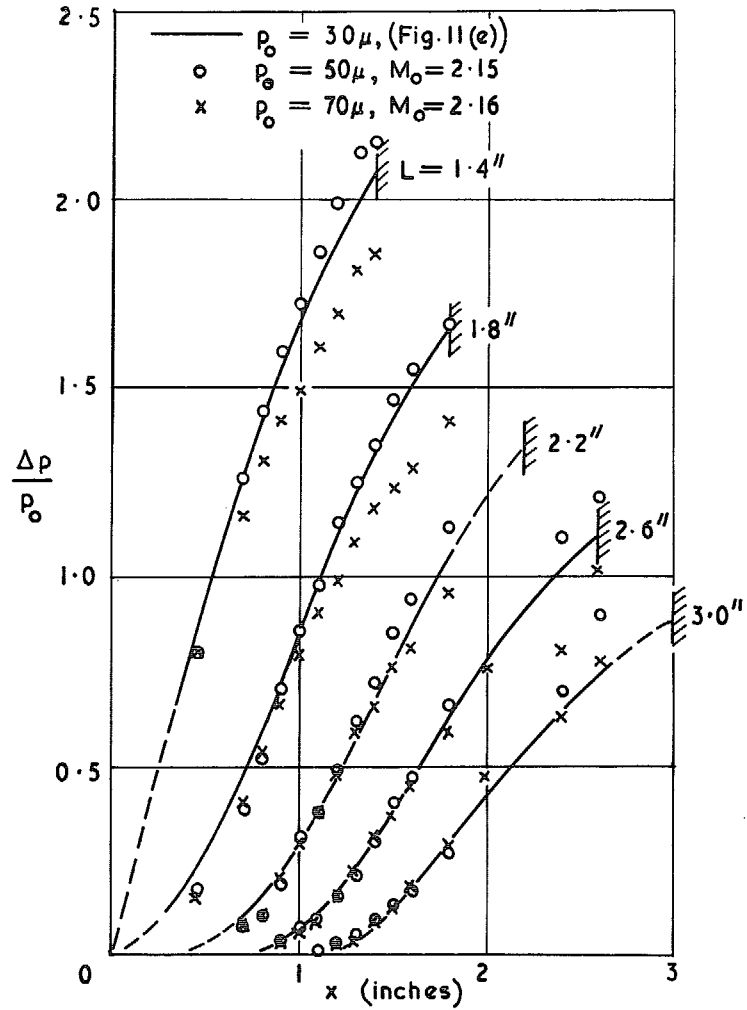
FIG. 13e. Effect of stream static pressure on incremental pressure distributions for $h = 0.5$in.
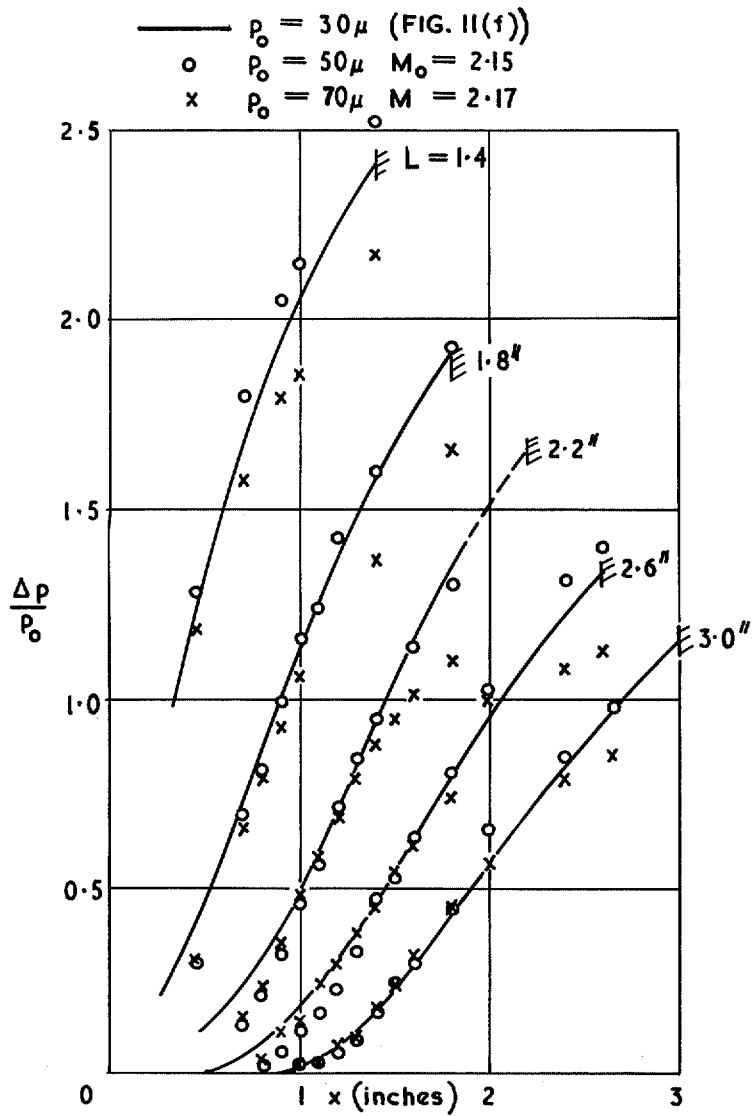
FIG. 13f. Effect of stream static pressure on incremental pressure distribution for $h = 0.6$in.
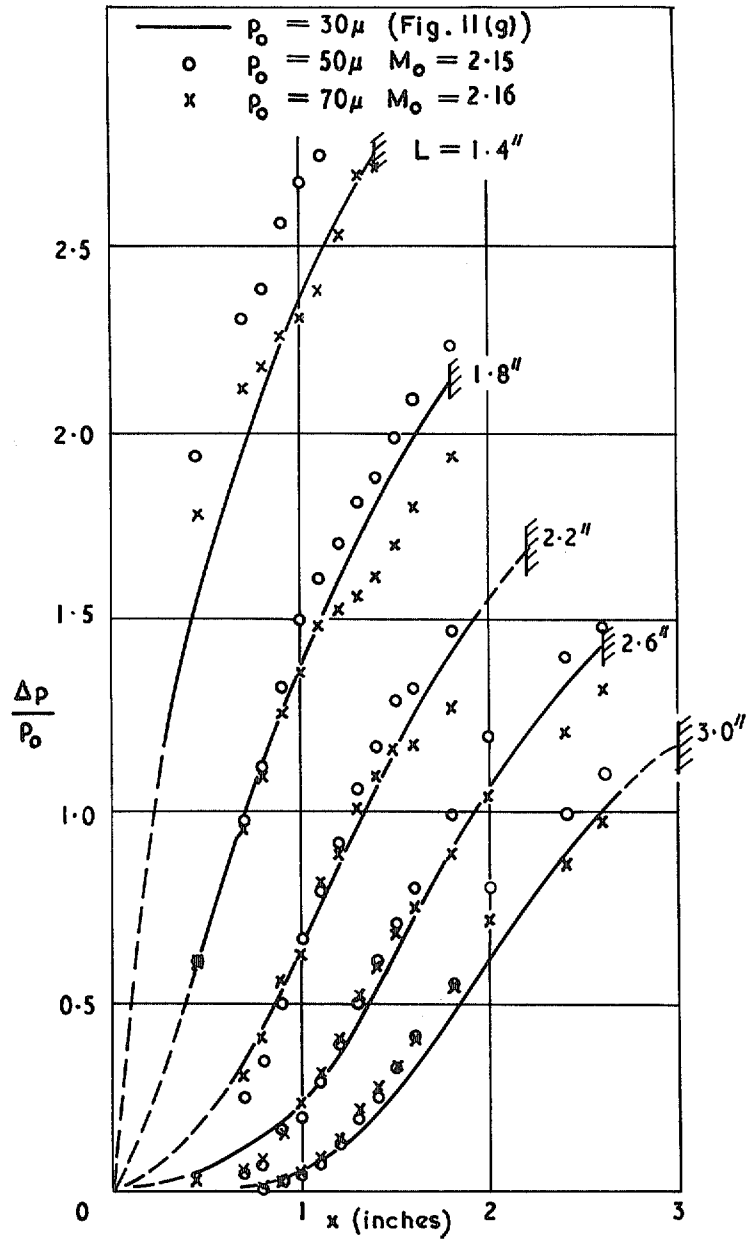
FIG. 13g. Effect of stream static pressure on incremental pressure distribution for $h = 0.7$in.
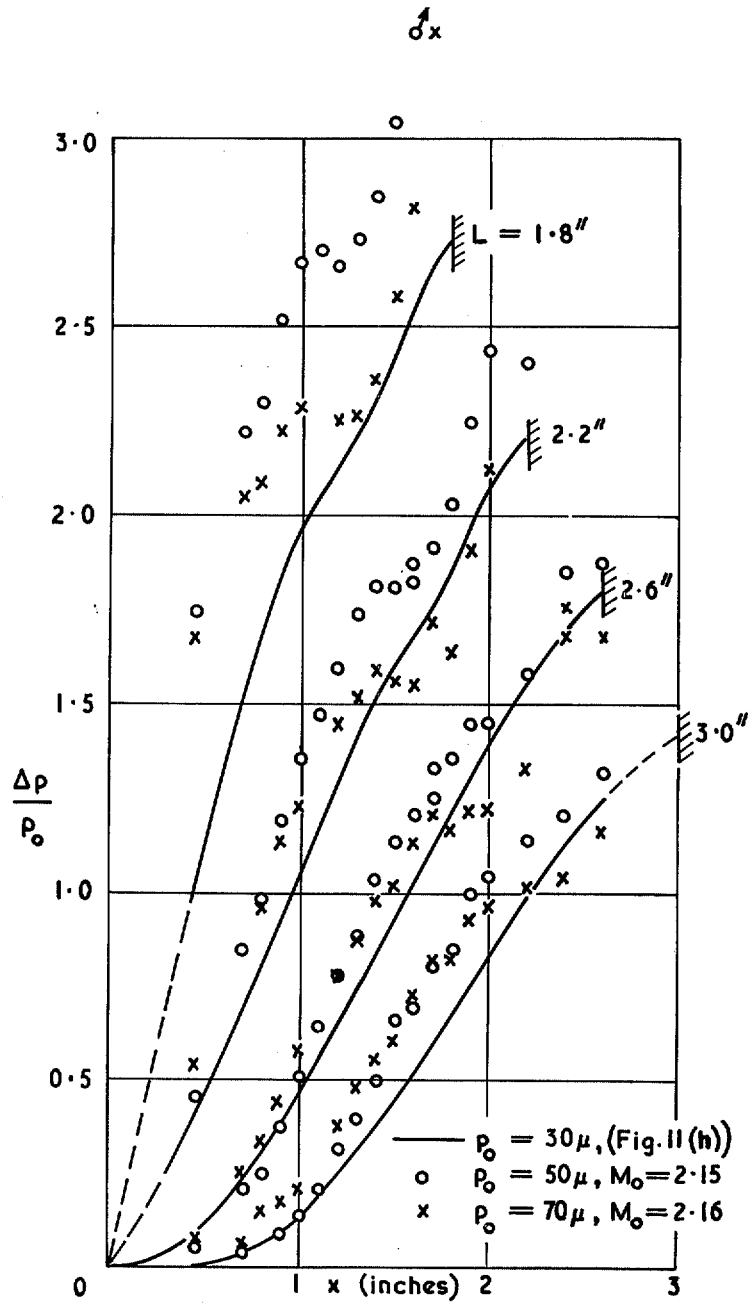
FIG. 13h. Effect of stream static pressure on incremental pressure distributions for $h = 0.9$in.
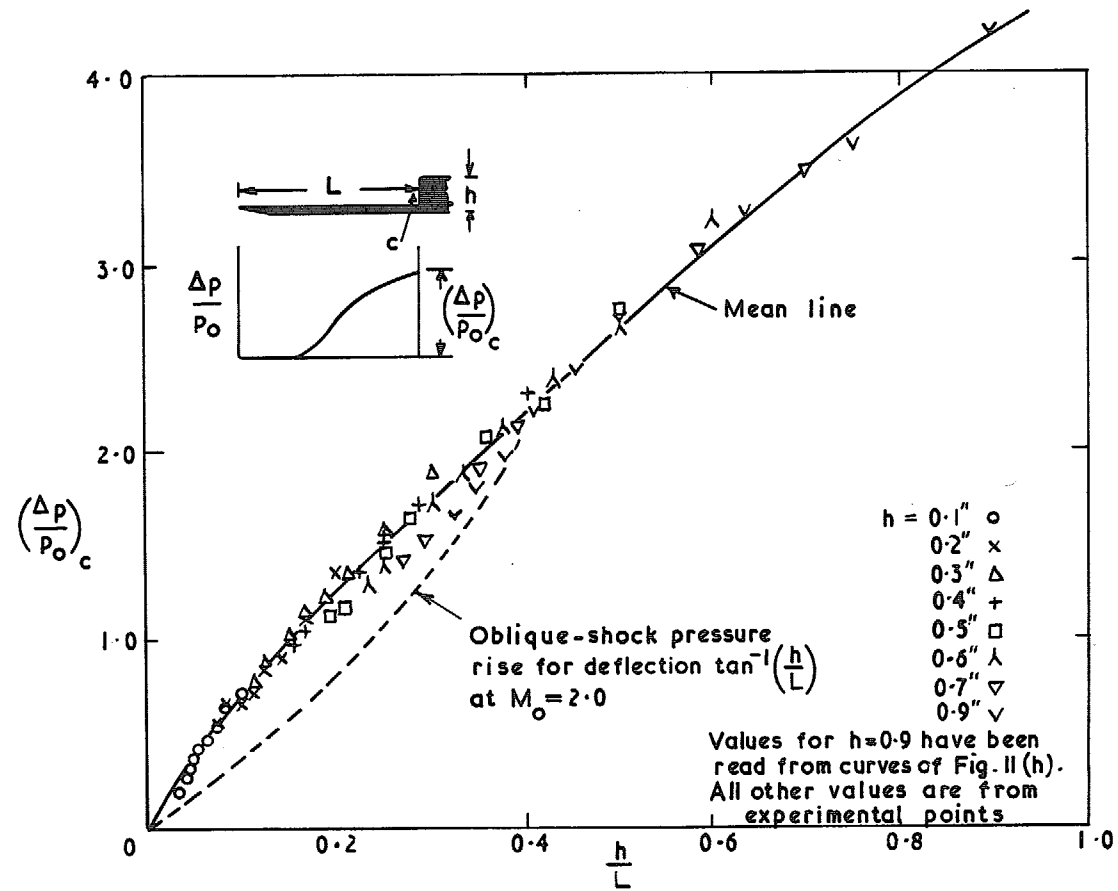
FIG. 14a. Correlation of corner pressure increment on basis of step geometry ($p_0 = 30\mu$, $1\cdot0$in. $\leqslant L \leqslant 2\cdot6$in.).
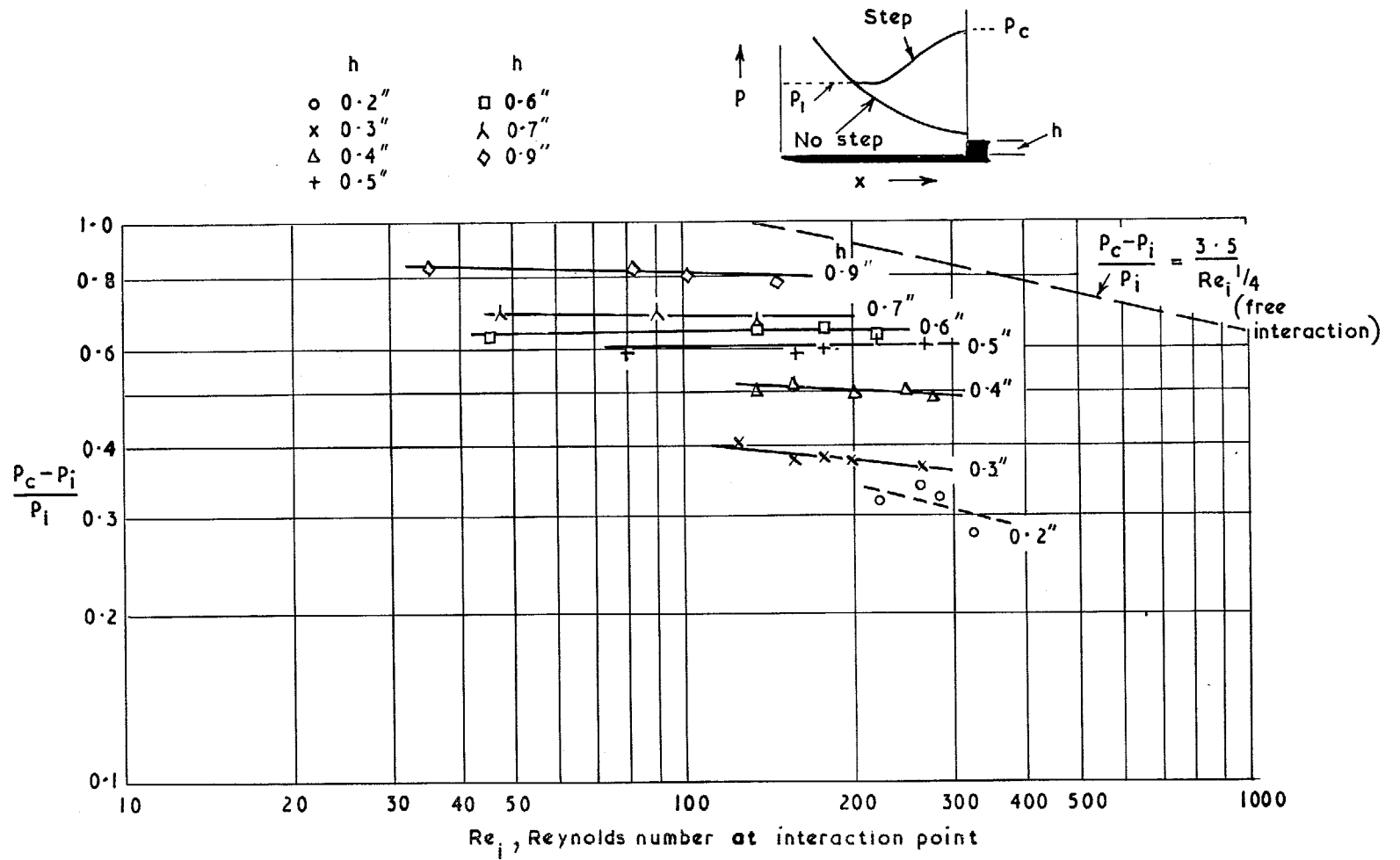
FIG. 14b.   Independence of pressure rise due to step from interaction-point conditions ($p_0 = 50\mu$).

37
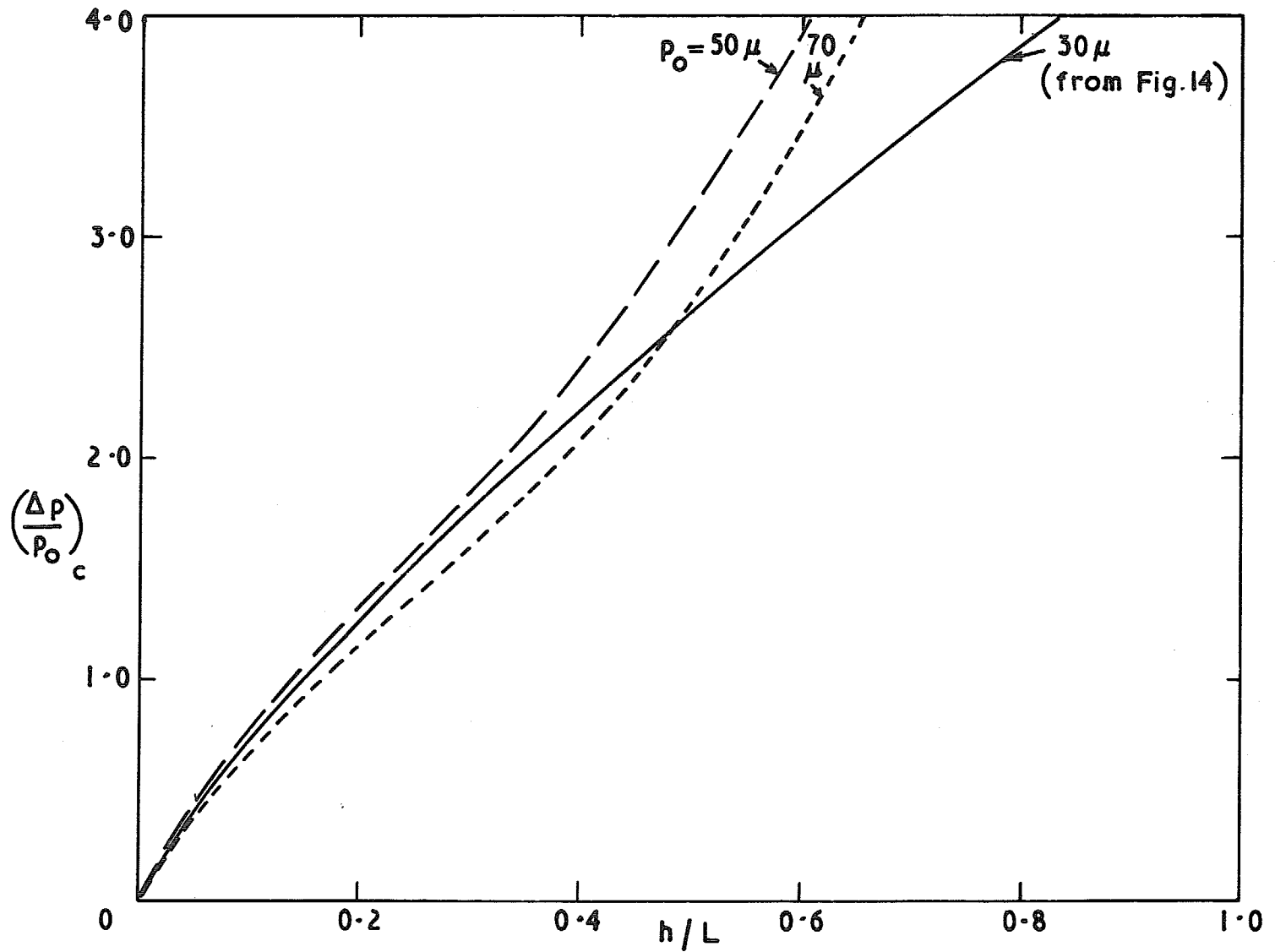
FIG. 15.   Influence of stream static pressure p_0 on mean lines of correlations similar to Fig. 14.
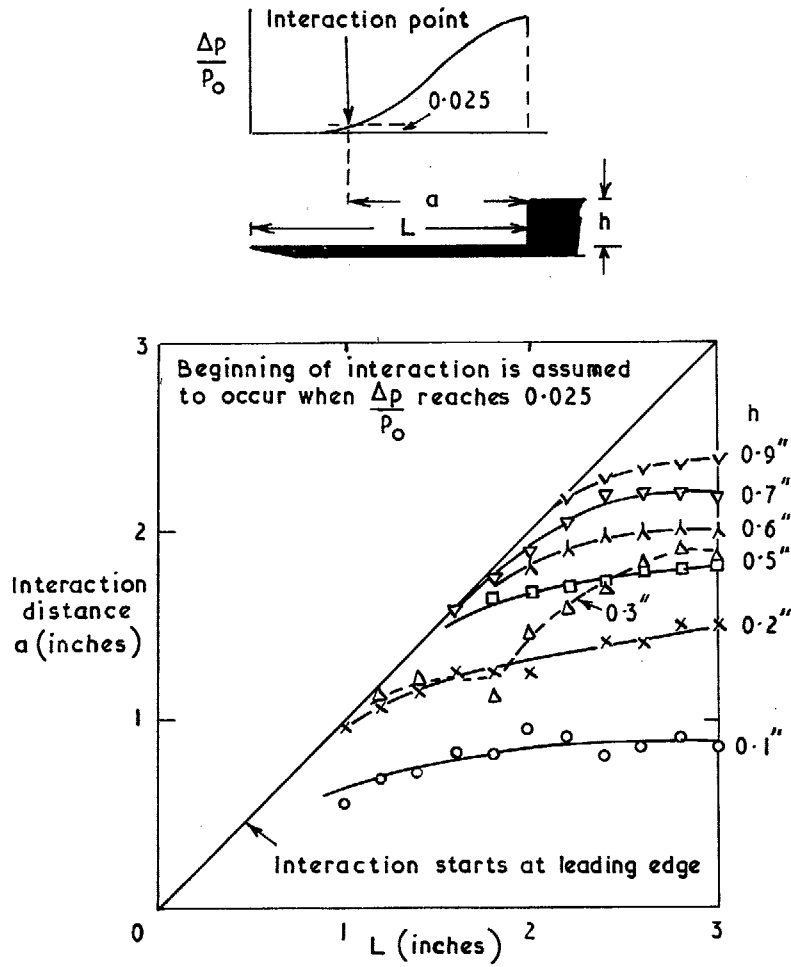
FIG. 16. Influence of step height and position on interaction distance, $p_0 = 30\mu$ $M_0 = 1.92$.
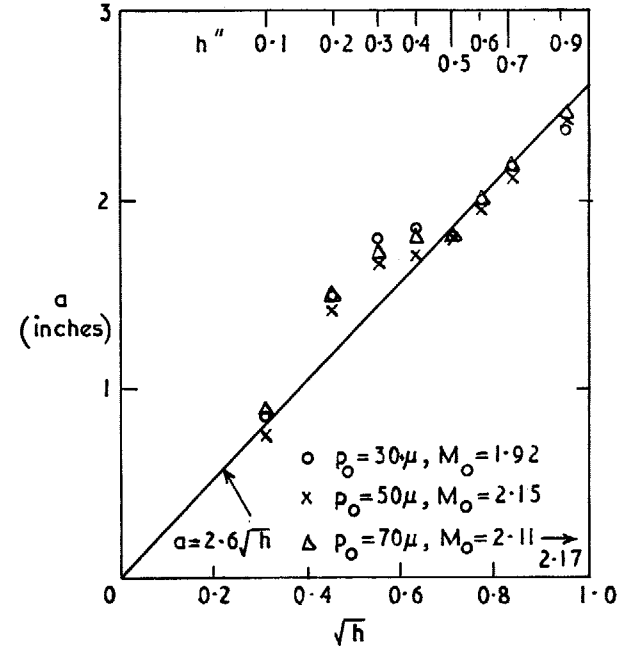
FIG. 17. Influence of stream static pressure on interaction distance for $L = 3.0$ in.

FIG. 18. Approximate correlation of complete incremental pressure distribution for $p_0 = 30\mu$, $L = 2\cdot6$in. and varying step heights.

FIG. 19. Approximate correlation of complete incremental pressure distributions at various values of L and h.

40
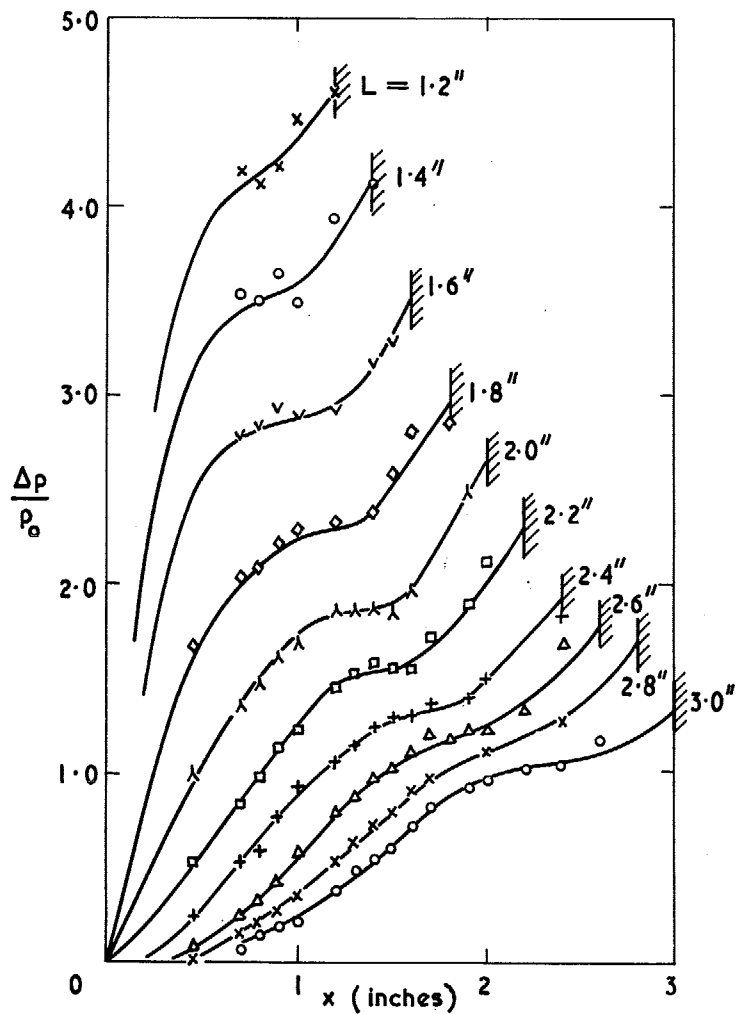
FIG. 20.   Kinked incremental pressure distributions for $h = 0.9$in., $p_0 = 70\mu$, $M_0 = 2.16$.
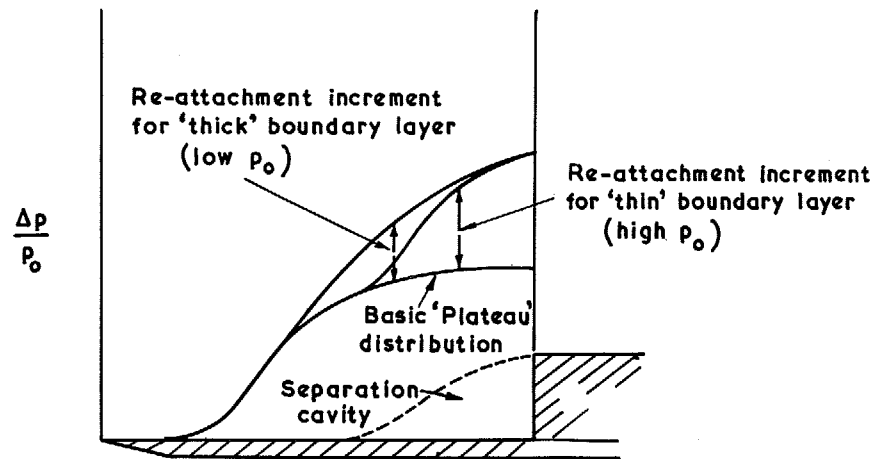
FIG. 21.   Possible effect due to upstream penetration of re-attachment pressure rise.

FIG. 22. (left figure)

200

Backward-facing
pitot-tube
touching plate

Cavity

150

Surface pressure in
absence of probe

100

P_s

Pressure
(μ)

{ Assumed point
  { of separation

50

Reading of backward-facing probe

0   1   2   3

x (inches)

42
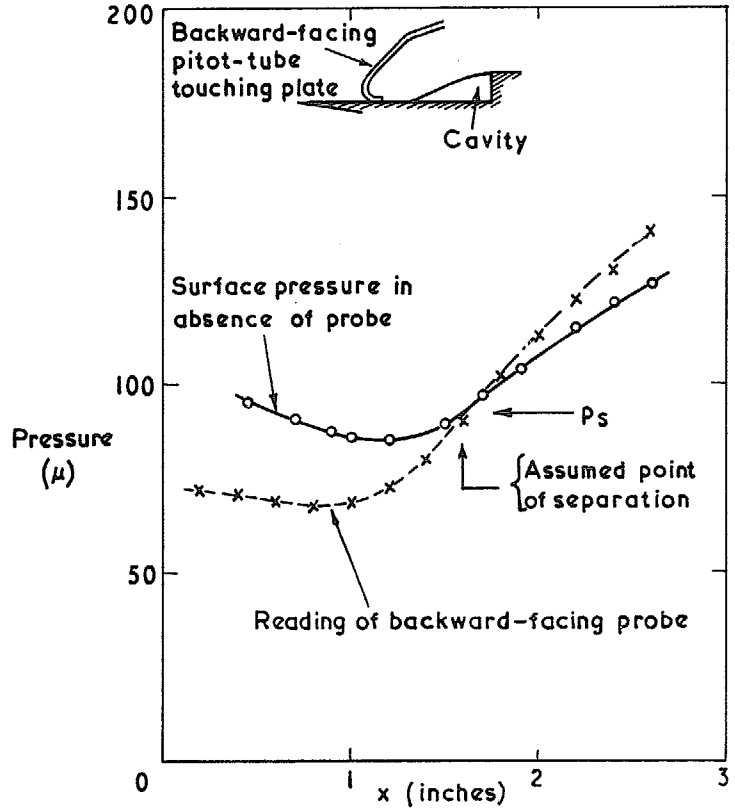
FIG. 22. Estimation of separation position from traverse of backward-facing probe ($p_0 = 70\mu$, $M_0 = 2.16$, $h = 0.5$in., $L = 3.0$in.).

FIG. 23. (right figure)

$M_o = 2.15$ and 2.16

$\overrightarrow{p_o} = 70\mu$

$\beta = 21.7^\circ$
19.7°
26.5°

h
$0.7''$
$0.5''$
$0.3''$

0   $1''$ $2''$ $3''$

$M_o = 2.15$

$\overrightarrow{p_o} = 50\mu$

$\beta = 24.8^\circ$
24.2°
β

$0.7''$
$0.5''$
$0.3''$

$M_o = 1.92$

$\overrightarrow{p_o} = 30\mu$

$\beta = 31.0^\circ$
35.6°

$0.7''$
$0.5''$
$0.3''$
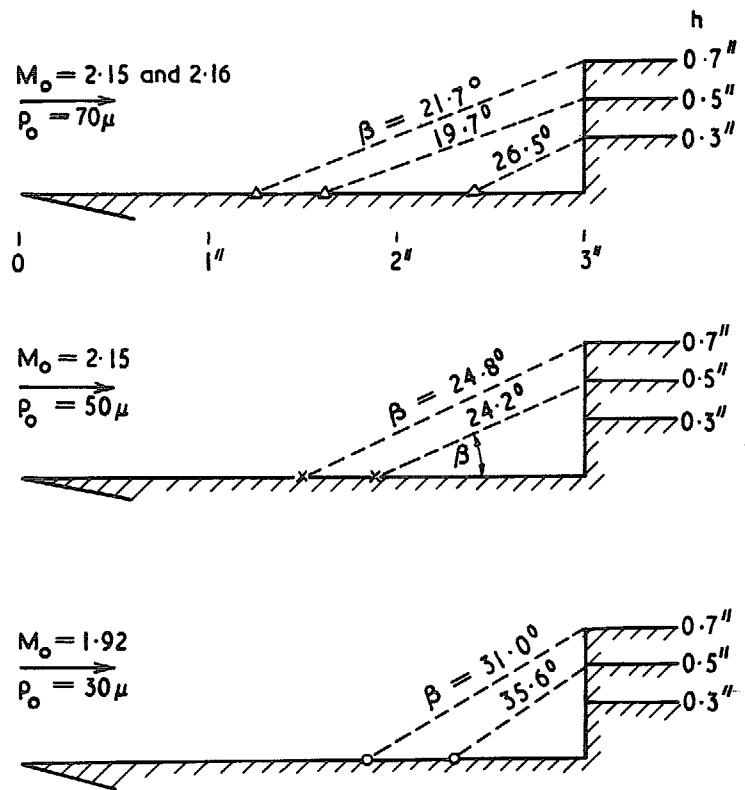
FIG. 23. Separation positions deduced from backward-facing pitot data ($L = 3.0$in.).
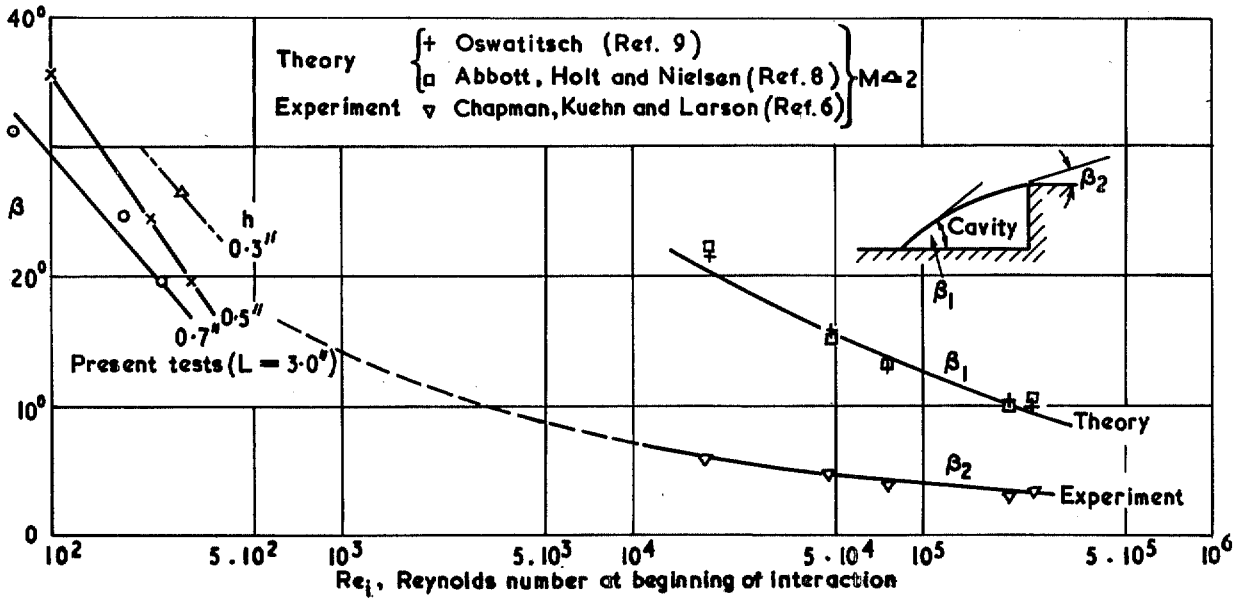
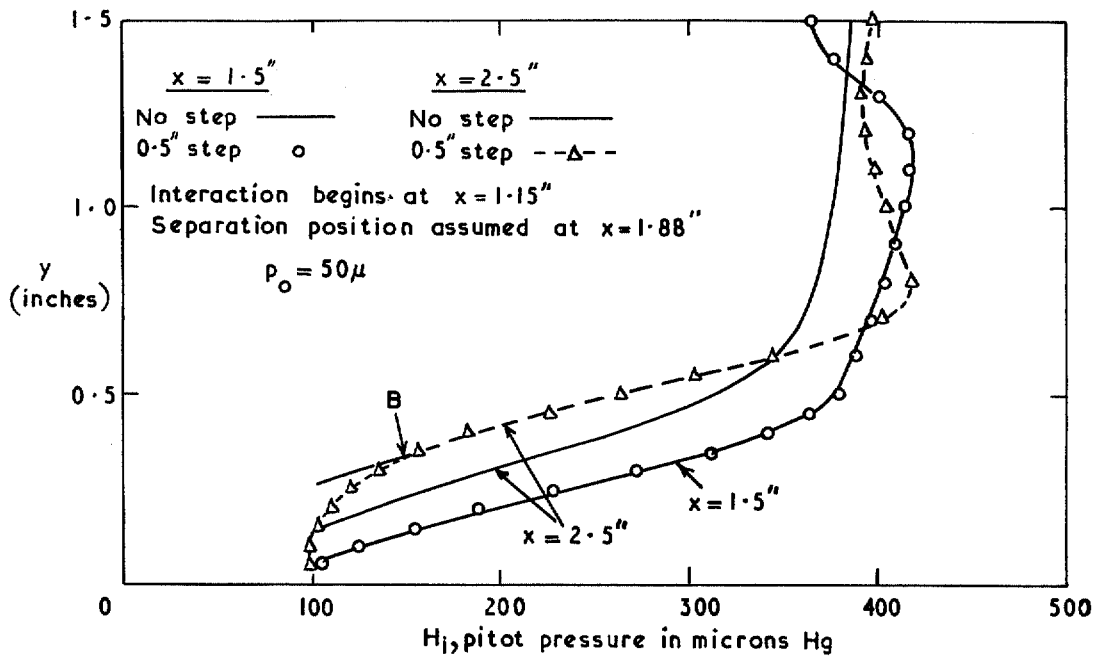FIG. 24.   Dependence of cavity angle β on interaction Reynolds number.

FIG. 25.   Effect of step on boundary-layer traverses at two chordwise positions ($p_0 = 50\mu$, $L = 3 \cdot 0$in.).

Cavity boundary defined by:-
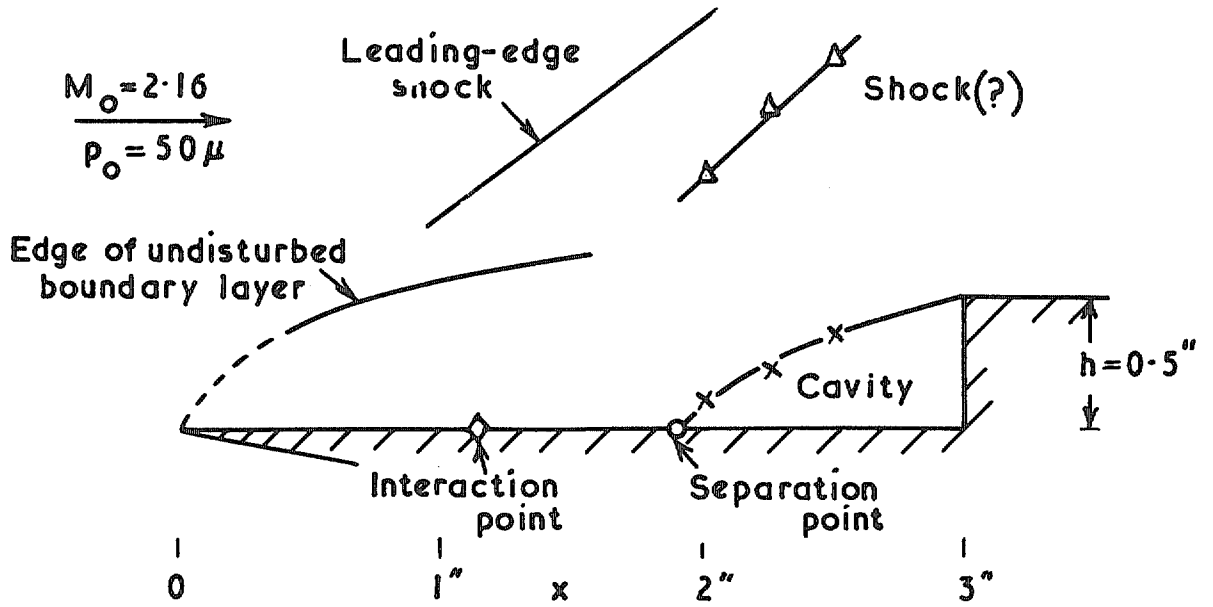o   from backward pitot
x   from pitot traverse (B in Fig. 25)

$M_o = 2 \cdot 16$

$p_o = 50 \mu$

Leading-edge shock

Shock(?)

Edge of undisturbed boundary layer

Cavity

$h = 0 \cdot 5''$

Interaction point

Separation point

0   1''   x   2''   3''

FIG. 26a.   Flow pattern ahead of step deduced from pitot-traverse data ($L = 3 \cdot 0$in., $h = 0 \cdot 5$in.).

44

$$M_o \simeq 2 \cdot 0$$

$$P_o = 23\mu$$

Bow shock

Boundary layer

0·9″ step
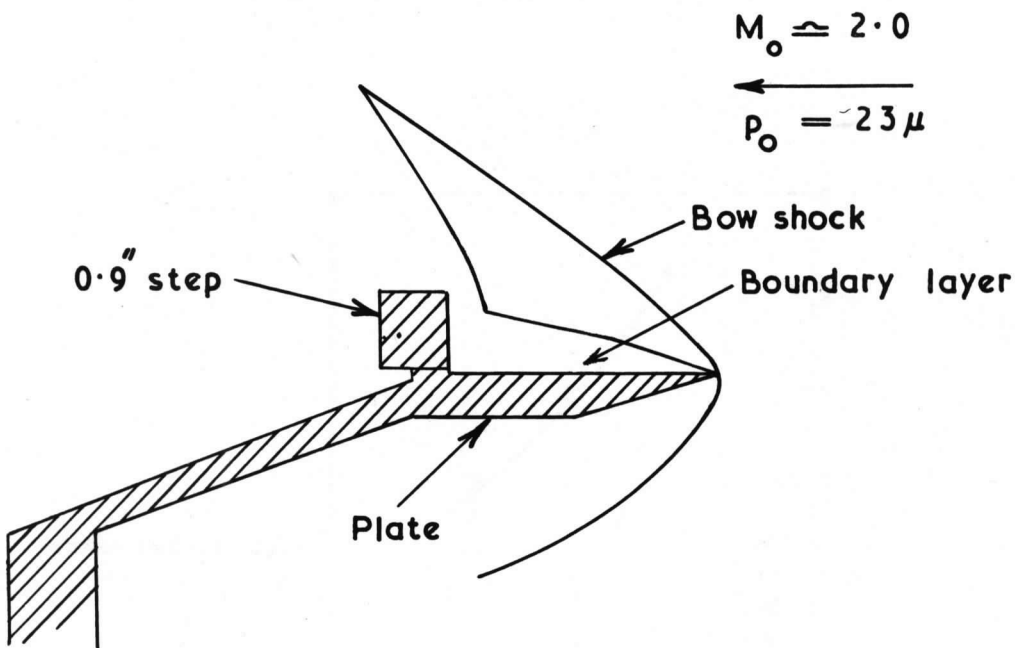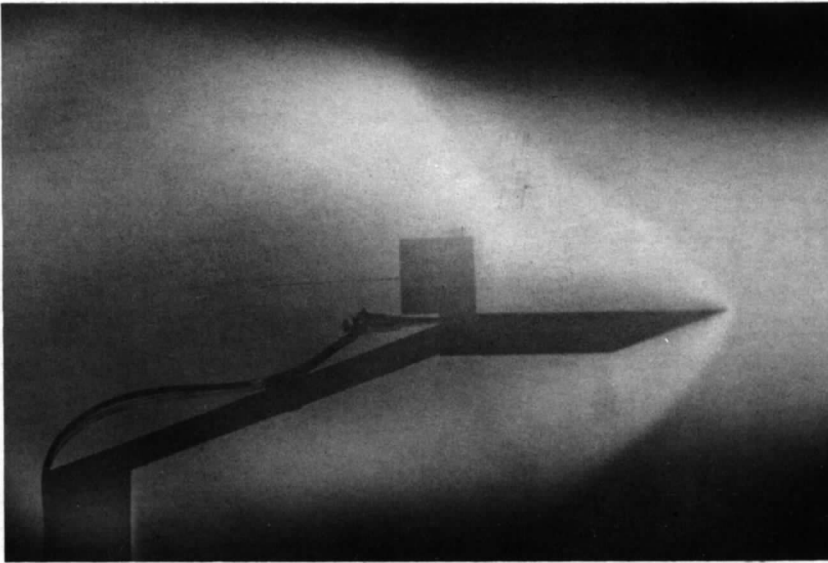
Plate

FIG. 26b.   Photograph of ionised argon flow past plate with 0·9 in. high step.
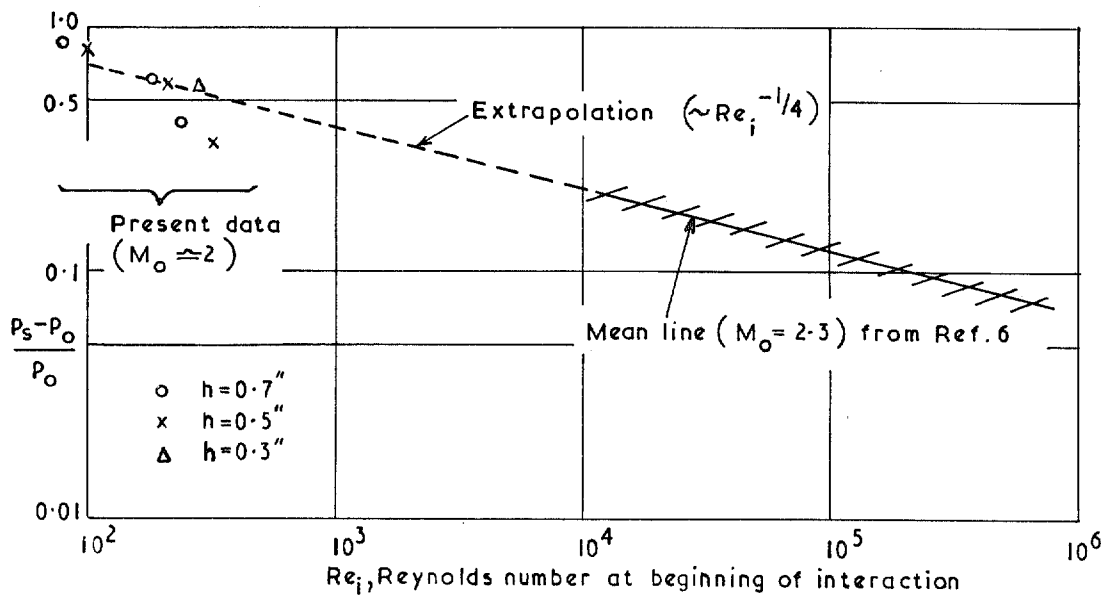
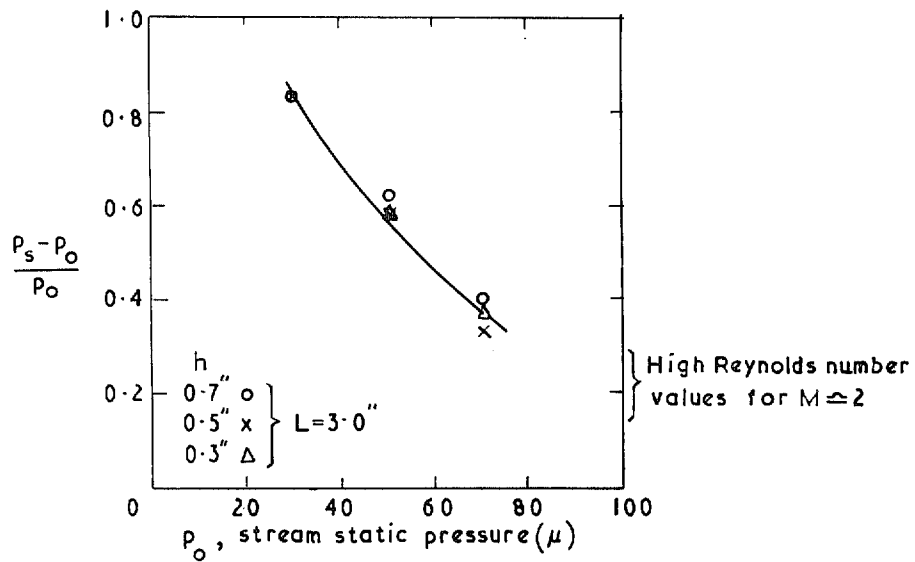FIG. 27.   Influence of Reynolds number on separation pressure rise.

FIG. 28.   Dependence of separation pressure rise on stream pressure level.

46